

# **Relative Localization using Satellite positioning**

KARL LUNDIN

Master in Systems, Robotics and Control

Date: December 6, 2019

Supervisor: Håkan Carlsson, Linnea Persson

Examiner: Joakim Jaldén

School of Electrical Engineering and Computer Science

Swedish title: Global och relativ GNSS-positionering



## Abstract

In this paper, the basis for Global Navigation Satellite Systems (GNSS) is presented and a comparison between the expected precision of the relative position between two receivers is presented based on observations made by two stationary receivers. The positioning is compared between the solution from two algorithms. The first relative estimate is based on making individual position estimates for the receivers and calculating the difference. The second uses a so called double difference method for estimating the relative position. The assumption is that systematic noises will be more successfully mitigated by the use of a double difference algorithm, which is also verified through simulations. The result of the observations is that the double difference performs slightly better, with a measured mean error of 4.8 and 4.9 m, compared to the relative position of the global estimates of 5.6 and 5 meters. These errors indicates that the random and unmodeled noises were larger in the sampling series than what was expected. A continued work should implement a filter that can lower the noise levels in the observations.

## Sammanfattning

I detta dokument presenteras grunderna för Satellitnavigation (GNSS) och en jämförelse mellan den förväntade precisionen hos den relativa positionen mellan två GNSS-mottagare baserat på mätningar från två stationära mottagare. Positioneringen jämförs för lösning som erhålls som differensen mellan individuella globala positioner samt när en differentierad positionslösning implementeras. Antagandet till grund för undersökningarna är att den differentierade estimatorn är bättre på att minska effekterna av systematiska brus. Detta verifieras även med hjälp av simulerings. Den positionslösning som erhålls visar att positionen baserat uteslutande på Satellitnavigation kan förväntas ligga på strax över 5 m, med uppmätta medelfel på 5 och 5,6 m, samt strax under 5 m för den dubbeldifferentierade estimatorn med uppmätta medelfel på 4,8 samt 4,9 m. Magnituden på felet indikerar att de omodellerade brusnivåerna var större än väntat. Ett fortsatt arbete bör söka att utveckla lösningen och implementera ett filter som kan minska brusnivåerna.

I would like to express my deepest gratitude to my supervisors Håkan Carlsson and Linnea Persson who I believe have gone well beyond their expected effort and invested a lot of time in aiding me in discussing the theory and investigating the implementation. I would also like to express a thank you to family and friends who have supported me through this project.

# Contents

<b>1</b>	<b>Introduction</b>	<b>1</b>
1.1	An introduction to Global navigation satellite systems . . . . .	1
1.2	Satellite orbits . . . . .	1
1.3	The idea of satellite navigation . . . . .	2
1.4	Applications of GNSS-positioning . . . . .	3
1.5	Other satellite navigation techniques . . . . .	3
1.6	Previous research . . . . .	4
1.7	Problem description and results . . . . .	5
1.8	Objective . . . . .	5
1.9	Scientific question . . . . .	6
1.10	Delimitation . . . . .	6
<b>2</b>	<b>Background</b>	<b>7</b>
2.1	Navigation frames and Earth representation . . . . .	7
2.1.1	Coordinate frame transformation . . . . .	8
2.2	The pseudorange signal and error terms . . . . .	9
2.2.1	Components of the pseudorange . . . . .	10
2.2.2	Pseudorange error terms . . . . .	11
2.3	Satellite positioning using ephemeris data . . . . .	12
2.4	Global positioning model and estimates . . . . .	13
2.4.1	Global positioning observation model . . . . .	16

2.5	Global positioning estimator model . . . . .	17
2.5.1	Weighted estimator . . . . .	18
2.5.2	Iterative steps of estimator . . . . .	19
2.6	Estimator pseudo-code . . . . .	20
2.7	Relative positioning . . . . .	21
2.7.1	Differential technique observation model . . . . .	21
2.7.2	Single difference technique . . . . .	22
2.7.3	Double difference technique . . . . .	22
2.8	Satellite Geometry . . . . .	24
<b>3</b>	<b>Method</b>	<b>27</b>
3.1	Global GNSS positioning . . . . .	27
3.1.1	Estimating satellite position . . . . .	27
3.1.2	Data extraction from sensor . . . . .	27
3.1.3	Experimental setup . . . . .	28
3.1.4	Global and relative positions from onboard estimate .	29
3.1.5	Global and relative position estimates from raw data .	29
3.2	Simulation of data . . . . .	30
3.2.1	Testing different error sources impact on global position	30
3.3	RMSE of relative position from global position and DD estimate . . . . .	31
<b>4</b>	<b>Results</b>	<b>32</b>
4.1	Error and convergence from simulated data . . . . .	32
4.1.1	Convergence of estimate for noise free measurements with different initial error . . . . .	33
4.1.2	Final estimate for added measurement noise of different magnitudes . . . . .	33
4.2	Calculating satellite position . . . . .	34
4.3	Position estimate using global positioning . . . . .	36

4.3.1	Position from onboard estimate . . . . .	37
4.3.2	Least square estimator from raw observation data . . . . .	38
4.4	Relative estimates . . . . .	45
4.4.1	Histograms of relative position and noise estimates . . . . .	45
4.5	RMSE of relative position from global positioning and DD estimate . . . . .	48
4.6	DOP values . . . . .	50
4.6.1	DOP values global estimates . . . . .	50
4.6.2	Double differenced DOP values . . . . .	51
<b>5</b>	<b>Conclusions and further work</b>	<b>56</b>
5.1	Results of simulations . . . . .	56
5.2	Precision of the estimates . . . . .	56
5.3	DOP values . . . . .	57
5.4	Further work . . . . .	57
.1	Least Squares and Probability . . . . .	57
.1.1	Least squares . . . . .	58
.1.2	Data structs and log format . . . . .	59

# **Chapter 1**

## **Introduction**

### **1.1 An introduction to Global navigation satellite systems**

The human presence in space began with the launching of the Soviet Union's Sputnik, closely followed by the USA's Explorer satellites in 1957 and 1958 respectively. Since then, many more launches of human-made objects into space have been performed, by several different countries. For the purpose of positioning there exists several systems in parallel, among them the US "Global Positioning System" (GPS), the Russian "Globalnaja Navigatsionnaja Sputnikovaja Sistema" [Latin transliteration] (GLONASS) and the Chinese 北斗 (Eng: Beidou) are arguably the most well known. The general name for those satellites used for navigation purposes is the "Global Navigation Satellite System" (GNSS).

### **1.2 Satellite orbits**

Some satellites used for e.g. radio and television are in an orbit around the earth at the same angular velocity as the planet's rotation, known as a geostationary orbit which implies that the satellite will stay over the same point on the surface of the earth. These satellites will travel along an orbit with a radius of 42.000 km or at a distance of around 36.000 km above the Earth's surface [1].

The GNSS satellites travel at a shorter distance and thus has a shorter orbit period. For the GPS system, the average distance is at 20.200 km which gives them a base orbit period of around  $\frac{1}{2}$  day. The other GNSS systems behave similarly to this. The distance to Earth is not constant over time since they will in practice always have some level of eccentricity, meaning that their path is elliptic with a center that may be far from the Earth's center. For navigation satellites, this eccentricity is generally small, below 0.02 meaning that the orbit is close to a circle [2].

### 1.3 The idea of satellite navigation

The process of determining a GNSS-receiver's position on earth is based on comparing its distance to a number of satellites whose position is known by the receiver in a process called trilateration. The idea is illustrated in an ideal and noise free 2-dimensional case in figure 1.1 for 2, 3 and 4 senders. The circles represent the radial distance to a satellite. For 2 senders, the solution is generally underdefined as multiple positions are valid. In a planar case that is illustrated with the two dots. In a 3D case, the solution space would form a circle at the intersections of the radius spheres. A unique solution only exists if both observations are equal to the corresponding radii and the circle collapses to a point. For three senders a unique solution is available and for four or more the system is overdetermined.

It is often preferred to write (small) numbers in text:  
 "For two senders, the solution [...]"

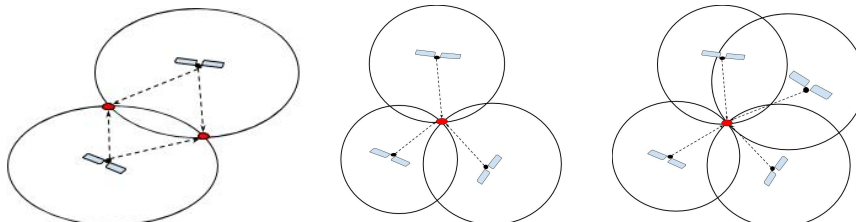


Figure 1.1: Example of positioning based on radial distance between sender and receiver for 2 (left), 3 (middle) and 4 (right) senders. The circles represent the distance from the sender and should be spherical, but is illustrated in 2D.

## 1.4 Applications of GNSS-positioning

The use of GNSS-positioning has spread from its original military purpose to being an integrated part of many applications, both business and consumer-oriented. The usage of positioning through satellite navigation is today widely spread and has numerous applications, such as being present in many modern cellphones, ships and cars. The advantages include its global usability for **outdoors** conditions as well as providing accuracy mostly within 5 meters at any time of the day [3].

In some applications, only the relative position between two units is of importance, e.g. for a ship docking or when landing on a platform. In this context the absolute position may be irrelevant and an offset from the true position does not influence the process, provided that both estimates contain the same offset. **The trivial method of getting a relative position given two global positions is to calculate the difference between.** If a very high precision of the relative estimate is required, meaning that the error in the relative position estimate must be very low, this method may be insufficient as the two **estimate errors** of individual global estimates may sum to a larger error. Then the use of some other technique which is better able to reduce the effect of the noise into the estimate may be superior to the trivial relative method. Different techniques have been developed to achieve a significantly higher precision than that available from standalone positioning. A few of these techniques will be presented in section 1.5.

In the future, the use of satellite positioning may become an even more integrated part of our society as the potential to obtain a position estimate correct to within a few **cm** may lead to revolutions in many industries. Two examples are farming, when tractors may work the field unsupervised virtually without overlap in its path [4] or the potential for autonomous delivery of medical or customer goods using drones [5].

## 1.5 Other satellite navigation techniques

Three techniques which build on the idea presented in section 1.3 worth describing briefly are the differential technique, Differential GPS (DGPS) and Real Time Kinematic (RTK).

Differential techniques are based on using the direction to a transmitter rather

than its position to estimate a relative distance between two points. The methods use that the scalar product between the direction vector and the relative distance is equal to the difference in distance to the transmitter. This way a relative position between two receivers can be calculated. Differential methods can be implemented as single, double or triple difference, where the use of double difference (DD) will be important in this paper.

DGPS is a form of differential technique where a base station with a known position is used for reference. The base station can then transmit correction factors for the satellite signals to the other receiver, called a rover.

The RTK method is a further development of the differential techniques, which utilizes the difference in phase between the signal for a base station and the mobile receiver. The wave length of the signal and the number of cycles between the positions is then calculated to obtain even higher precision.

## 1.6 Previous research

GNSS systems have been available for decades and much research has been performed on the behavior of the systems. Specifically on the topic of the DD technique, [6] shows an implementation of a weighted least squares solution based on the signal strength for a pair of stationary receivers on a rooftop. The error of the estimate is presented in relation to the true baseline, where for two different baselines of 3 m and 8 m respectively, an error of respectively 3.2 m and 3.6 m is presented.

In [7], similar techniques as in [6] is presented. One addition is that the estimates are performed in different environments with a 3 m baseline. For an open space environment, a mean error of 0.6-0.7 meter is achieved, for an environment with surrounding trees the measures mean error was 4 m and in the vicinity of buildings 2.3 m which indicate that noise levels in the observations may be very dependant on the environment.

In [8], the technique is presented with an error in position fix of less than 1 m error for the receiver positions. This is an example based on an experimental setup where any noise stemming from signal reflection can be expected to be zero as the receivers share the antenna between them.

In [9], the performance of DGPS is evaluated as a function of the distance to the base station. The results show that the position with 95% probability is correct to within 0.5-1 m near the base station and grows with 0.2 m per 100

km separation.

In [10] an RTK-solution is implemented and tested for baselines of 2-31 km, showing an accuracy of respectively 1 cm and 2 cm horizontally and vertically.

## 1.7 Problem description and results

This paper presents the work that has been done with producing a relative positioning for the GNSS-INS receiver provided by inertial sense. It is a multi-sensor unit where either measurements from a single sensor, or the fused information from several, can be extracted. The data from "MEMs gyros, accelerometers, magnetometers, barometric pressure, and GPS/GNSS is fused to provide optimal estimation"<sup>1</sup>. Data has been logged by sampling from stationary sensors and processed using MATLAB.

The results are based on the raw GNSS observation data sampled from the units and are presented in two ways: The relative position from the units from

- (i) A difference between individual position estimates.
- (ii) A Double Difference method.

The results show that for (i), the mean error can be expected to be in the magnitude of slightly above 5 m, with measurement mean values of 5 and 5.6 m. For (ii) the position error can be expected to be slightly below 5 m, with measurement mean values of 4.9 and 4.8 m. For a continued work a few improvements are suggested: data from other sensors may be fused to produce an even finer solution as well as the solution being produced in real-time. In addition to that, implementing a filter should be able to reduce much of the high frequency noise in the observations and lower the mean error.

## 1.8 Objective

The objective of this paper is to investigate the relative positioning estimate based on two different methods and compare them. The two algorithms which

---

<sup>1</sup><https://inertialsense.com/%C2%B5ins-dual/>

are implemented are to use the difference between the positions in the individual position estimates and the double-difference based relative position. The behavior is presented for uncertainty in position per direction and the calculated mean error.

## 1.9 Scientific question

The purpose of this paper is to investigate what precision in the positioning that can be expected from a GNSS-solution for the purpose of the automated landing process. This is reflected in the question, formulated below.

- What precision can be expected from a relative GNSS-solution between two receivers using difference in global position fix and differentiated methods.

Ideally an estimate that is correct to within one meter would ensure that the landing can be made safely.

## 1.10 Delimitation

Many applications, such as those mentioned above, are implemented as solutions to mobile problems. This investigation is limited to sampling from two receivers under stationary conditions, using a known distance. The results are also only presented for solutions presented from logged data. No real-time solution is implemented.

# Chapter 2

## Background

This section explains the theory and implementation of

- Important coordinate frames for representation and their relationship.
- How observations are made, modelled and the observation error sources.
- How satellite positions are calculated
- How a global position estimate and differenced relative estimates are calculated.
- How satellite geometry influences the estimate.

### 2.1 Navigation frames and Earth representation

In order to navigate in a 3D-world, a set of three vectors need to be defined. There exist global frames which may be used for positioning anywhere, as well as local frames which are defined with directions and origin at an arbitrary point. There are several representation frames for a point in a GNSS application, among those a few notable ones are the Longitude-Latitude-Altitude (LLA), Earth-Centered-Earth-Fixed (ECEF) and North-East-Down representations (NED). All systems presented follow the rotation of the earth. It is also implied that the standard is based on the WGS84 system as it is the basis for GPS.

**LLA:** The LLA-system is a spherical system, using the angular arguments degrees West of the Greenwich meridian, denoted  $\lambda$  and North of the equator, denoted  $\phi$ , as well as a straight coordinate height over the surface of the earth. The altitude argument relies on a reference to the model of the earth applied, where 0 altitude implies being on the surface.

**ECEF:** The ECEF system is a Cartesian system, where the x and y-axes go through the equator with the x-axis pointing through the 0-meridian and the z-axis straight north.

**NED:** A NED-coordinate system is defined locally at an arbitrary point such that the axes point respectively straight in the North, East and down direction, where down implies towards the center of the earth.

**Elevation Azimuth:** The Elevation-Azimuth system is a spherical system defined locally. The radius can also be introduced to turn it into a 3D system. Elevation implies the degrees above the horizon and Azimuth the degrees clockwise from the north direction. This works well for an origin at a low altitude as the zero degrees defined by the horizon will be perpendicular to the radial direction of the earth, but for a higher altitude the angle to the horizon will become negative and this frame may lose its utility.

### 2.1.1 Coordinate frame transformation

The different coordinate systems representations are illustrated in figure 2.1. The transformation between a point  $B$  in an ECEF frame to a local NED-frame around a point  $A$  is given by the matrix

$$\begin{bmatrix} n \\ e \\ d \end{bmatrix} = \begin{bmatrix} -\sin \phi \cos \lambda & -\sin \phi \sin \lambda & \cos \phi \\ -\sin \lambda & \cos \lambda & 0 \\ \cos \phi \cos \lambda & \cos \phi \sin \lambda & \sin \phi \end{bmatrix} \begin{bmatrix} \Delta x \\ \Delta y \\ \Delta z \end{bmatrix}$$

where  $n, e, d$  represents the position in the local frame,  $\lambda$  and  $\phi$  the longitude and latitude angles of the point of transformation and  $\Delta x, \Delta y, \Delta z$  the difference between points  $A$  and  $B$  in ECEF-coordinates.

A special case of the rotation matrix which is that of the earth's rotation around its own axis should be mentioned. As this rotation coincides with the ECEF z-axis, it is a planar rotation which using basic algebra can be proven to be

$$\begin{bmatrix} \cos \lambda & \sin \lambda & 0 \\ -\sin \lambda & \cos \lambda & 0 \\ 0 & 0 & 1 \end{bmatrix} \quad (2.1)$$

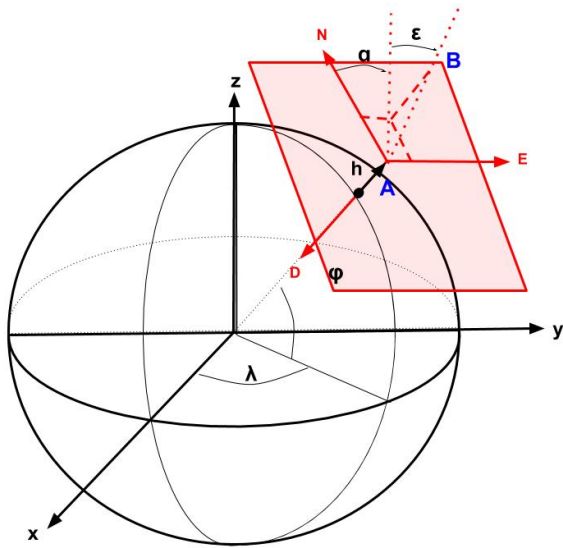


Figure 2.1: Commonly used coordinate frames for GNSS navigation and their correlation is shown. Global frames: ECEF, defined by directions  $x,y,z$ . LLA, defined by angles  $\lambda, \phi$  and height  $h$ . Local frames around a point  $\mathbf{A}$  where the plane in red is tangential to the surface: NED, defined by the directions  $\mathbf{N}, \mathbf{E}, \mathbf{D}$ , and Elevation Azimuth for a point  $\mathbf{B}$  with regards to point  $\mathbf{A}$  given by  $\alpha$  degrees clockwise from north and  $\epsilon$  degrees above the horizon.

for a clockwise rotation  $\lambda$ . A property of the rotation matrix is that for any matrix  $M(\lambda)$  defined by (2.1), the inverse rotation is equivalent to its transpose  $M(-\lambda) = [M(\lambda)]^T$ .

## 2.2 The pseudorange signal and error terms

The primary source of data for positioning is called the pseudorange and is based on calculating a time difference between transmission and reception which can be translated to a range through the speed of light. The specific method for measurement acquisition is based on sampling a sequence of the pseudorandom code sent out by a satellite, which is then compared for similarity to a longer sequence by the receiver. This gives the receiver information on when the signal was broadcast, while the time of reception is based on the receiver clock. Since in this project, the pseudorange will be sampled directly in the form of a distance from the receiver, the discussion on observation ac-

quisition will not be explained further, more information on the specifics of how the signal is sampled can be found in [2].

### 2.2.1 Components of the pseudorange

The pseudorange signal is measured as a time difference between time of transmission and reception. Both clocks times are assumed imperfect and containing an offset from the true time, which will impact the measurement. The measurement is considered a sum of three parts: the time difference between the true times of transmission and reception, the time difference between the respective clock offsets, and an error term [11]. The model for these clock offsets are discussed further in section 2.2.2.1. The measured time of propagation,  $T_{prop}$  is then expressed as

$$T_{prop} = (t_{rec} - t_{tr}) + (\Delta t_{rec} - \Delta t_{sat}) + \nu. \quad (2.2)$$

where  $t_{rec}$  and  $t_{tr}$  are the true times of reception and transmission,  $\Delta t_{sat}$  and  $\Delta t_{rec}$  the transmitter and receivers respective offset from the true time in seconds and  $\nu$  and error term, discussed further in section 2.2.2.2. The propagation time for the signal is, with previously mentioned orbit, at around 6~7 ms and is the sought after component of the signal since it tells the distance to the sender. The measurement is transformed to a distance through multiplying with the speed of light  $c$ , and an observation can instead be expressed as a function of the actual distance and clock difference as

$$y = \|\mathbf{p}^{sat} - \mathbf{p}_{rec}\| + c\Delta t + c\nu \quad (2.3)$$

where  $\mathbf{p}^{sat}$  and  $\mathbf{p}_{rec}$  are the positions of the sender and receiver respectively. The use of bold font, e.g.  $\mathbf{p}$  will be used forwards to indicate a vector.

The function  $h$  defined as

$$\begin{aligned} h(\mathbf{p}^{sat}, \mathbf{p}_{rec}, \Delta t_{rec}) &= \|\mathbf{p}^{sat} - \mathbf{p}_{rec}\| + c\Delta t_{rec} \\ &= \sqrt{((p_x^{sat} - p_x)^2 + (p_y^{sat} - p_y)^2 + (p_z^{sat} - p_z)^2)} + c\Delta t_{rec}. \end{aligned} \quad (2.4)$$

is introduced, turning equation (2.3) into

$$y = h(\mathbf{p}^{sat}, \mathbf{p}_{rec}, \Delta t_{rec}) - c\Delta t_{sat} + c\nu \quad (2.5)$$

$$= h(\mathbf{p}^{sat}, \boldsymbol{\theta}) - c\Delta t_{sat} + c\nu. \quad (2.6)$$

The argument  $\theta = [\mathbf{p}_{rec}, \Delta t_{rec}]$  has been introduced to represent the receiver state vector. The arguments of  $h$  are the primary variables to estimate, but before the method to obtain an estimate can be explained, more underlying theory must be presented.

## 2.2.2 Pseudorange error terms

The different components of the error term  $\nu$ , mentioned in section 2.2.1 are explained and given an expected range in this section. A summary of the noise sources can be found in table 2.1.

### 2.2.2.1 Clock errors

The clocks in satellites are very precise, but as many of them have been active for a long time, the error can still amount to large values due to error build up over a long time. This error is called a bias and originates in the clock time advancing slightly different from an ideal clock, called a drift. This drift can be modeled as a random walk behavior and means that the error tends to build up slowly over time. The bias in receivers can often be much larger with a much higher drift. However between two consecutive samples, the difference is small, e.g.: an average drift of +1 second/day translates to  $\sim 10\mu s/s$ . The clock biases give rise to a positioning error in two parts where the first part is the range error included in eq. (2.3). These biases should be taken into account since a clock error of 1 ms can result in a positioning error of thousands of kilometers as 1 ms of clock bias equals to  $c \cdot 0.001s \approx 3 \cdot 10^5$  m.

The second part of the clock bias positioning error stems from that the satellite position is determined with time as an argument, parametrized by a set of equations from the ephemeris data, explained more below. The receiver bias constitutes the largest part as an error in the receiver clock will lead to an error in the satellite position. The GNSS satellites travel at a speed of around 4000 m/s which means that a receiver clock error of  $\Delta t_{rec} = 0.01$  s can result in an error in the satellite position of around 40 m. Both the satellite and receiver clock errors will be compensated for, explained in section 2.3 and 2.5. The remaining error in the satellite clock after correction is in the range of 2.5 m [2].

### 2.2.2.2 Other error sources

The third part of the signal, the noise terms  $\nu$ , is composed of several parts. This can be split up into a common noise and non common noise, where a common noise implies that it is equal for two simultaneous observations separate in space. If the common noise is expressed it will be denoted  $\eta$ . Otherwise, it will be included in the unmodelled noise sources, denoted  $\epsilon$ .

The common noises include the Ionospheric and Tropospheric atmospheric noise, which can range up to 100 m [12] and 25 m [13] respectively, but mostly are in the range of about 5 m and 0.5 m respectively [2]. There are models for how to compensate for these effects, presented e.g. in [14] but they are not modeled in this project. Another common noise is the error in calculated position of the transmitting satellite, discussed further in section 2.3. The satellite position calculation is correct to an average 1 m in any direction [15].

The unmodelled noise sources include multipath effects which is when signals are reflected off other objects, as well as receiver noise. These noise sources can be expected to be in the range of 1 and 0.3 m respectively [2], but examples of multipath have been observed up to 100 m [14].

Noise Source	Range [m]
Satellite Clock	2.5
Satellite Orbit	1
Ionosphere	5
Troposphere	0.5
Multipath	1
Receiver error	0.3

Table 2.1: Noise sources in the range observations with a normal error range.

## 2.3 Satellite positioning using ephemeris data

In order to determine a receiver's global position using satellites, the satellite's position should be known. The satellite positions at a given time are accessible online in real-time, e.g. from [gnssplanning.com](http://gnssplanning.com) or can be calculated directly. The calculations are based on two parts: Almanac and ephemeris data. Almanac data is a predefined base orbit of lower accuracy which is up-

dated on an approximately daily basis which is readily available online, e.g. on <https://www.navcen.uscg.gov/> as well as satellites transmitting it directly. Precise positioning applications will rely on ephemeris data, which contains the parameters to calculate a more precise position of the satellite. This is transmitted by the individual satellite at a frequency of a few times per minute.

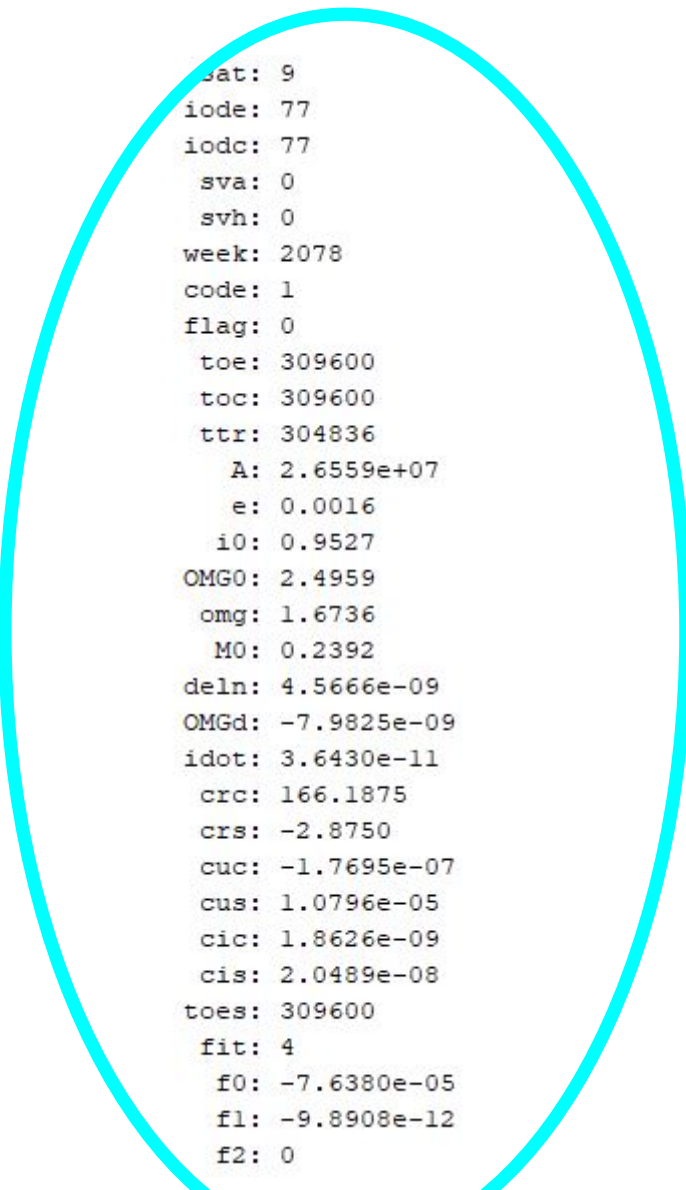
The data contained in the ephemeris message is based on the set of Keplerian equations which describes an orbit in space. Each message will contain information of 20 parameters: two reference times, three clock correction factors, six Keplerian parameters and nine perturbation parameters.

The clock correction factors are specific to each satellite and are the primary form of clock correction, used to correct for the  $\Delta t_{sv}$  term in (2.2). The equation to calculate the satellite clock bias, the precise algorithm for calculating the position and description of the Keplerian equations can be found in [16]. An example of the parameters in an ephemeris message used for this project is shown in figure 2.2. The satellite position is then calculated using the corresponding ephemeris data with time as an argument and will be given in an ECEF frame.

It is relevant to note that the time applied in the GPS-system is zeroed at Midnight January 6, 1980, and expressed in the format number of weeks and time of the week in seconds, using midnight Sunday-Monday as reference.

## 2.4 Global positioning model and estimates

As each measurement is only given in one dimension, signals from several transmitters need to be taken into account in order to estimate the receiver's position. To estimate a position in 3D as well as the receiver clock bias a minimum of 4 transmitting satellites is needed. Utilizing the pseudorange measurements in combination with knowledge of the satellite's position at the time of transmission, a position estimate can be calculated. The receiver and satellite position are  $3 \times 1$ -vectors  $[x, y, z]$  conveniently expressed in an ECEF frame, as that is how satellite positions are given in calculations presented in section 2.3. To solve this with regards to the currently unknown  $\theta$ , an iterative linearized solver can be implemented, presented below. For clarity, the values which are estimated and those calculated are as follows:



```

sat: 9
iode: 77
iodc: 77
sva: 0
svh: 0
week: 2078
code: 1
flag: 0
toe: 309600
toc: 309600
ttr: 304836
A: 2.6559e+07
e: 0.0016
i0: 0.9527
OMGO: 2.4959
omg: 1.6736
M0: 0.2392
dehn: 4.5666e-09
OMGd: -7.9825e-09
idot: 3.6430e-11
crc: 166.1875
crs: -2.8750
cuc: -1.7695e-07
cus: 1.0796e-05
cic: 1.8626e-09
cis: 2.0489e-08
toes: 309600
fit: 4
f0: -7.6380e-05
f1: -9.8908e-12
f2: 0

```

Figure 2.2: An example of a sample of the parameters contained in a single ephemeris message sampled on November 7, 2019.

**Estimates** The following are estimates in the model:

- $\mathbf{p}_{rec}$ : Receiver position in [m] (ECEF), vector  $1 \times 3$ .
- $\Delta t_{rec}$ : Receiver clock bias [s], scalar value.
- $\mathbf{p}^{sat}$ : Satellite position [m] at time of transmission (ECEF), vector  $1 \times 3$ .
- $\tau$ : Time of flight [s] for GNSS-signal, scalar value.

- $t$ : Observation time, seconds of week in GPS-time [s] that signal was received by the receiver, scalar value.
- $t_{tr}$ : Time of transmission [s], scalar value.
- $\gamma$ : Earth's rotation [rad] during signal time of flight, scalar value.

**Calculated or given values** These values are either given or directly calculated given values.

- $y$ : Pseudorange observation [m], scalar value.
- $\Delta t_{sv}$ : Satellite clock bias [s], scalar value.
- $t_{rec}$ : Nominal time of reception as registered by the receiver, not considering receiver clock bias, scalar value [s].
- $\xi$ : Ephemeris parameters, transmitted by each GNSS-satellite individually.
- $\epsilon$ : Unmodeled error source.

Any set of values or estimates will be ordered as a column vector, e.g.  $\mathbf{y}=[y^1 \dots y^n]^T$  is a  $n \times 1$  vector of pseudorange observation, where a superscript is used as an index to indicate corresponding satellite and observation.

**Satellite position** Satellite positions are calculated using the transmitted information in the ephemeris data as described in chapter 2.3. For a satellite, the position is calculated using only  $t$  as an argument, and parametrized by the ephemeris values in  $\xi$ :

$$\mathbf{p}^{sat}(t; \xi). \quad (2.7)$$

**Time of flight** The time of flight is the propagation time of a signal between two arbitrary points  $p_1$  and  $p_2$ . This is will be of relevance as the satellite position has changed between times  $t_{tr}$  and  $t$ . It is calculated as

$$\tau = \frac{1}{c} \|\mathbf{p}_1 - \mathbf{p}_2\| \quad (2.8)$$

**Time of transmission** Time of transmission for satellite signal is then calculated as

$$t_{tr} = t - \tau. \quad (2.9)$$

**Earth's rotation** The angle of rotation for a point on earth during  $\tau$  seconds is given by

$$\gamma = \tau \cdot \omega_e \quad (2.10)$$

**Rotated satellite position** Equations (2.7-2.10) allow for calculating the position of a satellite at  $t_{tr}$  as well as correcting for the rotation of the ECEF coordinate system during  $\tau$  seconds. The satellite position is calculated at  $t_{tr}$  and then rotated, resulting in the position  $\mathbf{p}'_{sat}(t_{tr}; \gamma)$  in ECEF-coordinates is given by applying a rotation matrix to the position  $\mathbf{p}_{sat}(t_{tr})$ .

$$\mathbf{p}'_{sat}(t_{tr}) = \begin{bmatrix} \cos(\gamma) & \sin(\gamma) & 0 \\ -\sin(\gamma) & \cos(\gamma) & 0 \\ 0 & 0 & 1 \end{bmatrix} [\mathbf{p}_{sat}(t_{tr})]^T \quad (2.11)$$

where the rotation applied is the counter clockwise rotation given by transposing (2.1).

**Satellite clock bias** The satellite clock bias is calculated at nominal time  $t_{rec}$  using the information in  $\xi$  and considered a constant for a single observation.

$$\Delta t_{sv}(t; \xi) \quad (2.12)$$

### 2.4.1 Global positioning observation model

A single observation  $y$  is modelled as

$$y = h(\mathbf{p}'_{sat}(t_{tr}), \boldsymbol{\theta}) - \Delta t_{sv} + \epsilon \quad (2.13)$$

which is the same as (2.5), with the exception that the satellite position is given by  $\mathbf{p}'_{sat}$ , given by equation (2.11) and  $\nu$  has been replaced by  $\epsilon$  to indicate that it is not modelled. Thus the full model of an expected observation  $\hat{y}$ , given satellite position and receiver states is given by

$$\hat{y} = ||\mathbf{p}'_{sat}(t_{tr}) - \mathbf{p}_{rec}(t)|| + c \cdot (\Delta t_{rec}(t) - \Delta t_{sv}) \quad (2.14)$$

where the unmodeled error  $\epsilon$  is omitted.

## 2.5 Global positioning estimator model

The purpose of the equations presented above is to reach a solution for the receiver states  $\mathbf{p}_{rec}$  and  $\Delta t_{rec}$ . The actual implementation is an iterative process where estimates are updated until convergence. For the sake of presenting the governing model, any variable should be interpreted as the current estimate, which will then be updated at the next iteration until convergence is attained. For a set of  $n$  observations  $\mathbf{y}$  and the corresponding satellite positions  $P^{sat}$  which is a  $3 \times n$  matrix, equation (2.5) can be expressed as:

$$\mathbf{y} = h(P^{sat}, \boldsymbol{\theta}) + \Delta t_{sv} + \epsilon \quad (2.15)$$

$$= \begin{bmatrix} h^1(\mathbf{p}^{(1)}, \boldsymbol{\theta}) \\ \vdots \\ h^n(\mathbf{p}^{(n)}, \boldsymbol{\theta}) \end{bmatrix} + \begin{bmatrix} \Delta t_{sv}^1 \\ \vdots \\ \Delta t_{sv}^n \end{bmatrix} + \begin{bmatrix} \epsilon_1 \\ \vdots \\ \epsilon_n \end{bmatrix} \quad (2.16)$$

The satellite clock errors  $\Delta t_{sv}$  will be subtracted from the equations using the equation in [16] to get

$$\mathbf{y}' = h(\mathbf{p}^{sat}, \boldsymbol{\theta}) + \epsilon \quad (2.17)$$

$$= \begin{bmatrix} h^1(\mathbf{p}^{(1)}, \boldsymbol{\theta}) \\ \vdots \\ h^n(\mathbf{p}^{(n)}, \boldsymbol{\theta}) \end{bmatrix} + \begin{bmatrix} \epsilon_1 \\ \vdots \\ \epsilon_n \end{bmatrix} \quad (2.18)$$

The equations are solved for the estimate  $\hat{\boldsymbol{\theta}}$  such that the error

$$\|\mathbf{y}' - h(P^{sat}, \boldsymbol{\theta})\|^2 \quad (2.19)$$

between observations and expected observations are minimized

$$\hat{\boldsymbol{\theta}} = \underset{\boldsymbol{\theta}}{\operatorname{argmin}} (||\mathbf{y}' - h(P^{sat}, \boldsymbol{\theta})||^2). \quad (2.20)$$

The system of equations is solved using the gradient of the equations. The gradient of the observation model equation (2.14) is for a satellite  $i$

$$\begin{aligned} \frac{\partial}{\partial \boldsymbol{\theta}} h^{(i)}(\mathbf{p}^{(i)}, \boldsymbol{\theta}) &= \frac{\partial h(\mathbf{p}^{(i)}, \boldsymbol{\theta})}{\partial x} + \frac{\partial h(\mathbf{p}^{(i)}, \boldsymbol{\theta})}{\partial y} + \frac{\partial h(\mathbf{p}^{(i)}, \boldsymbol{\theta})}{\partial z} + \frac{\partial h(\mathbf{p}^{(i)}, \boldsymbol{\theta})}{\partial \Delta t} \\ &= -\frac{p_x^{(i)} - p_x}{\|\mathbf{p}^{(i)} - \mathbf{p}\|} - \frac{p_y^{(i)} - p_y}{\|\mathbf{p}^{(i)} - \mathbf{p}\|} - \frac{p_z^{(i)} - p_z}{\|\mathbf{p}^{(i)} - \mathbf{p}\|} + c \\ &:= \nabla h^{(i)}(\mathbf{p}^{(i)}, \boldsymbol{\theta}) \end{aligned} \quad (2.21)$$

All the gradients described by (2.21) are collected in a  $n \times 4$  matrix  $H$ :

$$H(P^{sat}, \boldsymbol{\theta}) = \begin{bmatrix} \nabla h^1(\mathbf{p}^1; \boldsymbol{\theta}) \\ \vdots \\ \nabla h^n(\mathbf{p}^n; \boldsymbol{\theta}) \end{bmatrix}. \quad (2.22)$$

The result of (2.22) leads to the least square solution of (2.20) being described by:

$$\hat{\boldsymbol{\theta}} = (H^T \cdot H)^{-1} H^T \mathbf{y}', \quad (2.23)$$

as described in .1.1. Equation 2.23 is a step in a Gauss-Newton iterative process where a step is expressed as

$$\begin{aligned} \boldsymbol{\theta}^{(j+1)} &= \boldsymbol{\theta}^{(j)} - \hat{\boldsymbol{\theta}} \\ &= \boldsymbol{\theta}^{(j)} - (H^T(\boldsymbol{\theta}^{(j)}) H(\boldsymbol{\theta}^{(j)})^{-1} H^T(\boldsymbol{\theta}^{(j)})(\mathbf{y} - h[P^{sat,(j)}, \boldsymbol{\theta}^{(j)}])) \end{aligned}$$

where the superscript  $(j)$  indicates an iteration number.

### 2.5.1 Weighted estimator

If there is knowledge of the uncertainty in the observations, the minimizing function in 2.20 can be described by

$$\hat{\boldsymbol{\theta}} = \underset{\boldsymbol{\theta}}{\operatorname{argmin}} \left( \|\mathbf{y} - h(P^{sat}, \boldsymbol{\theta})\|_W^2 \right). \quad (2.24)$$

where  $\|\mathbf{X}\|_W^2 = \mathbf{X}^T W \mathbf{X}$  and  $W$  is a matrix of weights, here it will always be assumed diagonal and non-negative. **The so-called Best Linear Unbiased Estimator (BLUE) solution to equation (2.23) will then be expressed as**

$$\hat{\boldsymbol{\theta}}_{BLUE} = (H^T W H)^{-1} H^T W \mathbf{y} \quad (2.25)$$

As described in .1.1.1.

In [17], the signal-to-noise-ratio (SNR) value, which is closely related to the CNR and is recorded by the receivers is used as an estimate of the magnitude of the noise, such that the weight matrix will be described as a diagonal matrix  $W = \operatorname{diag}(w_1, \dots, w_n)$  for  $n$  observations. A weight  $w_i$ , corresponding to observation  $y^{(i)}$  and its corresponding registered SNR $^{(i)}$  value in dBHz are calculated as

$$w_i = 10^{-0.1 \cdot SNR^{(i)}} \quad (2.26)$$

## 2.5.2 Iterative steps of estimator

The calculations to obtain (2.20) is in the order:

1. Calculate all  $\Delta t_{sv}$  for the satellites at time of reception  $t$  and adjust the observations  $\mathbf{y}' = \mathbf{v} - \Delta t_{sv}$ . This step is not repeated.

put this above

An epoch will be used to describe a set of observations made at the same instance and will be denoted by  $[k]$ . The final estimate, meaning the last iteration of the state estimates, will be denoted  $\boldsymbol{\theta}[k]$ . For the first epoch,  $k = 1$ . The initial estimate of the receiver states  $\boldsymbol{\theta}_0[1]$  is set to zero, i.e.  $\mathbf{p}_{rec}^{(0)}[1] = [0, 0, 0]$  and  $\Delta t_{rec}^{(0)}[1] = 0$ . For the subsequent epochs,  $k > 1$ , the final estimate of the previous epoch is used as initial estimate, i.e.  $\boldsymbol{\theta}_0[k + 1] = \boldsymbol{\theta}[k]$ .

2. Adjust the observation for the receiver clock bias  $\mathbf{y}'' = \mathbf{y}' - c\Delta t_{rec}$ .

For each satellite individually:

3. Calculate signal time of flight  $\tau^{(i)} = \frac{(\mathbf{y}^{(i)})''}{c}$ .
4. Calculate the satellite positions  $\mathbf{p}^{(i)}(t_{rec} - \tau^{(i)}; \xi)$ .
5. Calculate the rotation angle  $\gamma^{(i)}$ .
6. Adjust the satellite position as in (2.11) to obtain  $(\mathbf{p}^{(i)})'_{sat}(t_{tr})$ .
7. Calculate  $\hat{\boldsymbol{\theta}}$  from  $\mathbf{p}'(t_{tr})$ ,  $\mathbf{y}''$  and  $\boldsymbol{\theta}$  as in equation (2.23) or (2.25).

This is continued until convergence for steps 2-7, where the convergence threshold has been set to  $10^{-3}$  m, indicating that

- The variables  $\mathbf{y}''$ ,  $\tau$ ,  $\mathbf{p}_{rec}$  and  $\Delta t_{rec}$  all are interdependent.
- $\mathbf{p}_{sat}$ , is dependant only on  $\Delta t_{rec}$  and  $\tau$ .
- $\gamma$  is dependant only on  $\tau$ .
- $t$  is dependant only on  $t_{rec}$  and  $\Delta t_{rec}$ .

Du har nu både pseudokod och en lista, en räcker antagligen.

## 2.6 Estimator pseudo-code

For the first epoch, the initial values of the receiver  $\theta_0[1]$  are set to 0. For any succeeding epoch  $k > 1$ , the initial estimate of the states  $\theta_0[k]$  will use the final estimate of the previous epoch  $\theta[k - 1]$ .

To calculate the receiver states during one epoch, all the estimated values are dependent on each other and any calculation will use the values calculated in the previous iteration of the others as input. In the code, the last iteration is denoted with a hat symbol, e.g.  $\hat{p}_{rec}$  and superscript is indexed by  $(\hat{i})$ .

The function "estimate\_satellite\_clock\_bias" is that from equation (2.12). "get\_satellite\_position" comes from equation (2.7). The rotation matrix in (2.11) is represented by  $R$  and the "estimate\_position" function is the least squares solution to (2.23).

In the following pseudo-code, the set of satellite positions  $P_{sat}$  is a  $n \times 3$  matrix, for a set of  $n$  satellites where an index  $j$  relates to the corresponding satellite position  $p^{(j)}$ . It is assumed that the set  $\Xi = \{\xi^{(1)}, \dots, \xi^{(n)}\}$  contains only the ephemeris data of the active satellites in each epoch.

```

1. Calculate satellite clock bias at observation time for each satellite
for all j in  $\Xi$  do
     $\Delta t_{sv}(j) \leftarrow \text{estimate\_satellite\_clock\_bias}(t, \Xi(j))$ 
end for

2. Adjust the observations for  $\Delta t_{sv}$ 
for all j in  $\Xi$  do
     $y(j) \leftarrow y(j) - c\Delta t_{sv}(j)$ 
end for

 $\Delta p \leftarrow 100$ 
 $\Delta b \leftarrow 100$ 

3. Iterate until convergence: calculate receiver states
while  $(|\Delta p| \cup |\Delta b|) > 0.1$  do
    3.1 Calculate signal time of flight
    for all j in  $\Xi$  do
         $y(j) \leftarrow y(j) - c\Delta t_{rec}$ 
         $\tau(j) \leftarrow y(j)/c$ 
    end for
    3.2. Calculate the satellite position, rotation and rotated position
    for all j in  $\Xi$  do
         $P_{sat}(j) \leftarrow \text{get\_satellite\_position}(\Xi(j), t - \tau(j))$ 
         $\gamma(j) \leftarrow \omega_e \cdot \tau(j)$ 
    end for

```

Vad är unionen av skalärer?

```

 $P_{sat}(j) \leftarrow R(\gamma(j)) \cdot P_{sat}(j)$ 
end for
3.3 Estimate  $p_{rec}$  and  $\Delta t_{rec}$ 
 $\hat{p}, \hat{\Delta t}_{rec} \leftarrow \text{estimate\_position}(P_{sat}, \mathbf{y}, p_{rec}, \Delta t_{rec})$ 
 $dp \leftarrow p_{rec} - \hat{p}$ 
 $db \leftarrow \Delta t_{rec} - \hat{\Delta t}_{rec}$ 
 $p_{rec} \leftarrow \hat{p}$ 
 $\Delta t_{rec} \leftarrow \hat{\Delta t}_{rec}$ 
end while

```

As it is a linearised system, the values of  $\mathbf{y}, \tau, \mathbf{p}^{sat}, \gamma, p_{rec}$  and  $\Delta t_{rec}$  will be updated per each iteration. This implies that for each iteration the position and receiver clock bias are estimated, and in turn the satellite position is adjusted for the updated clock bias value. This is repeated until convergence is reached.

## 2.7 Relative positioning

Relative positions can be calculated through the difference in positions calculated as in section 2.5.2 above. In this section a relative estimate using a DD-method is presented. The idea is to create an estimate of the relative distance between two positions by using the shared information between two receivers. It is based on that for two unit vectors  $\mathbf{u}_a^{(i)}$  and  $\mathbf{u}_b^{(i)}$  both pointing from receivers  $a$  and  $b$  respectively at position  $\mathbf{p}_a$  and  $\mathbf{p}_b$ , to the same satellite at position  $\mathbf{p}^{(i)}$  are considered to be parallel, as the angle  $\alpha$  between  $\mathbf{u}_a^{(i)}$  and  $\mathbf{u}_b^{(i)}$  is very small. The idea is presented in figure 2.3. This is motivated by that the satellite distance is generally much larger than the distance between any two points on earth, e.g. an isosceles triangle where the two receivers at a distance of 1 km and the satellite at a distance of  $2 \cdot 10^7$  m result in  $\alpha$  being smaller than  $0.05^\circ$ . The threshold for two observations considered close is set to 10 ms. If the observations are separated by more than that the entire epoch is discarded.

Long complex sentence, make shorter and simplify

### 2.7.1 Differential technique observation model

For the differential techniques presented below, the equation for a pseudorange measurement for the two receivers and a shared satellite  $i$ , at a given epoch will

be:

$$y_a^i = \rho_a^{(i)} + c(\Delta t_a - \Delta t^{(i)}) + \eta_a^i + \epsilon_a^i \quad (2.27)$$

$$y_b^i = \rho_b^{(i)} + c(\Delta t_b - \Delta t^{(i)}) + \eta_b^i + \epsilon_b^i \quad (2.28)$$

where  $\rho_a^{(i)}$  indicates the distance between a satellite  $i$  and receiver  $a$ .

## 2.7.2 Single difference technique

In single difference technique, illustrated in figure 2.3, the difference between two receivers is calculated, based on their relative distance to a satellite  $i$ , shown below when subtracting equation (2.28) from (2.27):

$$\begin{aligned} \Delta y_{ab}^i &= y_a^{(i)} - y_b^{(i)} \\ &= \rho_a^{(i)} + c(\Delta t_a - \Delta t^{(i)}) + \eta_a^i + \epsilon_a^i \\ &\quad - \rho_b^{(i)} + c(\Delta t_b - \Delta t^{(i)}) + \eta_b^i + \epsilon_b^i \\ &= (\rho_a^{(i)} - \rho_b^{(i)}) + c(\Delta t_a - \Delta t_b) - (\eta_a^i - \eta_b^i) + (\epsilon_a^i - \epsilon_b^i) \\ &= \Delta \rho_{ab}^{(i)} + c \Delta t_{ab} + \Delta \eta_{ab}^i + \Delta \epsilon_{ab}^i \end{aligned}$$

As presented in [18], with the same notation of  $\Delta$  signifying a difference, **this enables for the elimination** of the satellite clock bias and orbit error, as well as atmospheric interference being effectively removed for receiver separations less than 30 km. Receiver clock bias should still be estimated.

## 2.7.3 Double difference technique

In order to remove the receiver clock bias, double difference can be implemented, illustrated in figure 2.4. This relies on the difference between two satellites,  $i$  and  $j$ , common between the two receivers. Introducing the symbol  $\nabla$  to signify double difference, the equations is set up as

$$\begin{aligned} \nabla \Delta y_{ab}^{ij} &= \Delta y_{ab}^{(i)} - \Delta y_{ab}^{(j)} \\ &= \Delta \rho_{ab}^{(i)} + c \Delta t_{ab} + \Delta \epsilon_{ab}^{(i)} - \Delta \rho_{ab}^{(j)} - c \Delta t_{ab} - \Delta \epsilon_{ab}^{(j)} \\ &= \Delta \rho_{ab}^{(ij)} + \Delta \epsilon_{ab}^{(ij)}. \end{aligned} \quad (2.29)$$

In equation (2.29) the **receivers** clock bias is eliminated. The atmospheric noise has been omitted as explained in section 2.7.2. Further, the relation

between the relative position of two receivers is the dot product along a unit vector  $\mathbf{e}^i = [e_x, e_y, e_z]$  pointing to a satellite  $i$ :

$$\Delta y_{ab}^{(i)} = \mathbf{e}^i \cdot \mathbf{r}_{ab}$$

and similarly, with a reference satellite  $j$ , the double difference distance is given by

$$\nabla \Delta y_{ab}^{(ij)} = (\mathbf{e}^i - \mathbf{e}^j) \cdot \mathbf{r}_{ab} + \Delta \epsilon_{ab}^{(ij)}.$$

Thus, given a set of  $n + 1$  unit vectors pointing towards **as many different satellites**, and their corresponding pseudorange measurements, a solution can be found utilising equation (2.23). Using satellite  $j$  as reference, with its corresponding direction unit vector and observation as reference gives the following vectors

$$H = \begin{bmatrix} \mathbf{e}^1 - \mathbf{e}^j \\ \vdots \\ \mathbf{e}^n - \mathbf{e}^j \end{bmatrix}, \quad \nabla \Delta \mathbf{y}_{ab}^{(j)} = \begin{bmatrix} \Delta y_{ab}^{1j} \\ \vdots \\ \Delta y_{ab}^{nj} \end{bmatrix}. \quad (2.30)$$

Equation 2.30 may be solved using the same least square method of 2.23 as the global position, but with the updated direction matrix.

**Weighted least squares** In [6] it is also suggested to use a **BLUE estimator** with the CNR in dBHz, denoted  $\psi$ , as an estimate of the noise level. The CNR value is registered by the receivers individually and is assumed inversely proportional to the variance of the noise of the observation  $\sigma^2$ . **A higher variance shall result in a lower weight, formulated as that the variance of the noise for an observation between satellite  $i$  and receivers  $a$  and  $b$  is given by**

$$\begin{aligned} (\sigma^{(i)})^2 &= (\sigma_a^{(i)})^2 + (\sigma_b^{(i)})^2 \\ &\propto (\psi_a^{(i)})^{-2} + (\psi_b^{(i)})^{-2}. \end{aligned}$$

The weight matrix  $W$  is proposed as a diagonal weight matrix expressed as

$$W = \text{diag} \left( \frac{(\psi_a^1)^2 \cdot (\psi_b^1)^2}{(\psi_a^1)^2 + (\psi_b^1)^2}, \dots, \frac{(\psi_a^n)^2 \cdot (\psi_b^n)^2}{(\psi_a^n)^2 + (\psi_b^n)^2} \right) \quad (2.31)$$

and the optimal solution is calculated as

$$\hat{\boldsymbol{\theta}}_{\text{BLUE}} = ((H^{(j)})^T W H^{(j)})^{-1} (H^{(j)})^T W \nabla \Delta \mathbf{y}_{ab}^{(j)}$$

as proposed in equation (2.25), and  $(H^{(j)})$  and  $\nabla \Delta \mathbf{y}_{ab}^{(j)}$  are those presented in equation (2.30). Reference satellite  $j$  is chosen to be the signal with the highest CNR value for each epoch. For these cases notable increase in accuracy is shown, compared to that of two global position estimates.

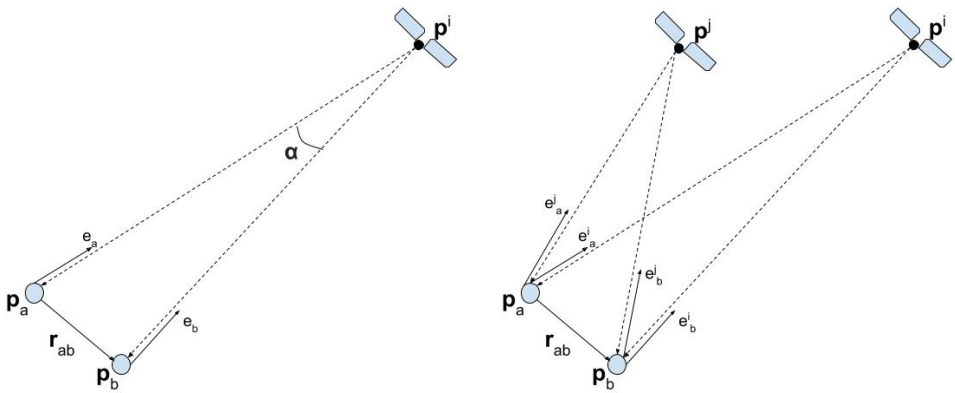


Figure 2.3: Single difference technique is able to estimate a relative position as well as eliminating satellite clock bias.

Figure 2.4: Satellite double difference can be calculated using two different satellites shared between the receivers

## 2.8 Satellite Geometry

One important aspect of the accuracy is in the spread of the satellites the receiver can obtain data from. If all observable transmitting satellites appear in a high angle over the horizon - as can be the case in an urban environment with many tall buildings - the accuracy can be expected to decrease compared to a case with more spread out satellite constellation. As all observations measure a distance in one direction, if all observable satellites are positioned close to being in the same direction, then distance estimates in other directions become poor. This is illustrated for an artificial 2D case in figure 2.5 and is an effect of that close-lying points on a plane perpendicular to the radius all are approximately at the same distance from the center.

In relation to this, the dilution of precision (DOP) can be defined. This is a matrix quantifying the geometric distribution of the satellites in use. Defining the matrix  $Q = (H^T H)^{-1}$ , where  $H$  is the Jacobian of the geometric matrix in (2.18) gives an estimate of the uncertainty of the solution per direction based on the geometry of the observed satellites.  $q_{ij}$  is used to describe element row

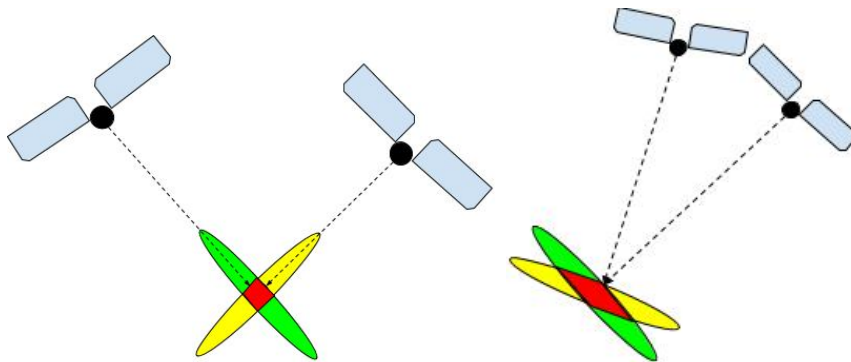


Figure 2.5: Illustration of the accuracy based on satellite constellation. Areas of high probability perpendicular to each satellite intersect, with the high probability intersection area marked in red. In the left image the angles between the satellites is large creating a small region, while in the right image the small angle yields a larger area.

and column, the following definitions are commonly observed:

$$HDOP = q_H = \sqrt{q_{11}^2 + q_{22}^2} \quad (2.32)$$

$$VDOP = q_V = q_{33} \quad (2.33)$$

What is the value, mean error, maximum error, standard deviation, variance?

$$(2.34)$$

$$TDOP = q_T = q_{44} \quad (2.35)$$

$$GDOP = q_G = \sqrt{q_{11}^2 + q_{22}^2 + q_{33}^2 + q_{44}^2} \quad (2.36)$$

Assuming that the geometric matrix is given in local NED coordinates, the HDOP, VDOP and PDOP respectively correspond to the horizontal, vertical and position uncertainty. TDOP is an estimate of the uncertainty in  $\Delta t_{rec}$  and GDOP the geometric uncertainty. This gives an estimate of how noise in the observation maps to an error in the respective estimate. For this, the noise of each individual satellite should be assumed of equal magnitude [19]. E.g. given a VDOP value of 3 and an error in the observations of 1 m, discussed in section 2.2, can be expected to result in a vertical error of 3m.

The relation between satellite geometry and actual position uncertainty is expressed as a product of the noise level times the corresponding DOP value.

$$\sigma_X = \epsilon \cdot q_X \quad (2.37)$$

The actual noise level in the observations, the sum of all error sources dis-

cussed in section 2.2, called the User Equivalent Range Error (UERE), is however usually not known to the receiver.

The theoretically greatest achievable vertical spread is found with satellites under the receiver. This will not be achievable unless receiver is at a very high altitude since satellites below the horizon can't be observed. **In practice an elevation threshold of at least  $10^\circ$  should be implemented since observations from low satellites have a higher noise level [20].**

This leads to that the horizontal spread is mostly much greater than the vertical and the HDOP-value can be expected to be smaller than the VDOP-value by a factor up to  $\sim 2.5$  [21]. A GDOP value of 1 is considered ideal and should be considered good up to about 6 [22].

# Chapter 3

## Method

### 3.1 Global GNSS positioning

#### 3.1.1 Estimating satellite position

Does this section need to be here?

To verify that the satellite trajectories are correct the satellite positions are calculated for a given time span using the method described in section 2.3 from the received ephemeris data. This is then compared to the historical satellite positions available on-line<sup>1</sup>. Plots showing the trajectory, as well as elevation and azimuth for a given time frame are produced and compared in section 4.2.

#### 3.1.2 Data extraction from sensor

The INS unit allows for data sampling and streaming in real-time as well as logging for post-processing through three different types of software. A GUI called EvalTool is available from the producer Inertial Sense<sup>2</sup> for logging data for most applications, both fused and unfused data from the GNSS-receiver and the IMU units. In addition to that, there is a command-line tool called CL Tool for logging of much the same functionality<sup>3</sup>. However, for the sake of this project, unprocessed pseudorange observation data from the receivers were required to implement and compare the single and double-difference

<sup>1</sup>e.g. <https://in-the-sky.org/> and <https://www.gnssplanning.com/#charts>

<sup>2</sup><https://inertialsense.com/>

<sup>3</sup><https://docs.inertialsense.com/>

methods described in chapter 2.7. In order to extract those, data must be parsed directly from the Software Development Kit (SDK) projects available. A logger, producing comma-separated values (.csv)-type log files of the received packages is available at <https://github.com/Kallemange/Communications> for post-processing. More information on the logger and data structures in use can be found in appendix .1.2.

### 3.1.3 Experimental setup

In order to test the receiver's behavior over time, two receivers are placed stationary at a baseline of 10 m pointing first in N-direction as well as in E-direction, with measurements taken for approximately 30 minutes in Ugglevikskällan, a glade in the forest on coordinates: 59.353°N, 18.073°E, shown in figure 3.1. One receiver was placed close to the pin indicated in the figure, and the other positioned east and south of it. The directions were set using a

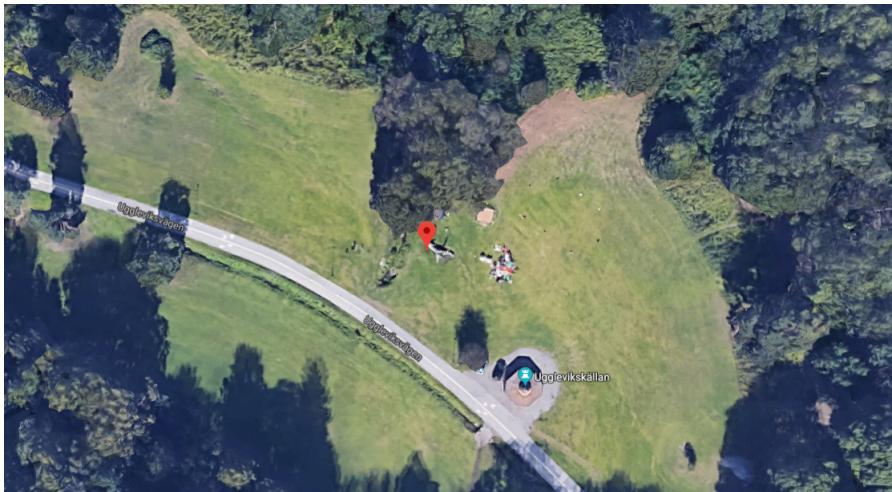


Figure 3.1: Uggleviken, place where observations were made. Image taken from Google Maps: <https://www.google.com/maps>

digital compass on an android phone and the distance through using a measuring tape. The logger is started for the receivers separately, but are connected to the same computer where the log files are stored.

### 3.1.4 Global and relative positions from onboard estimate

The processed estimates from the onboard electronics are sampled and logged in parallel to the raw data. This contains information on the global position in an ECEF or LLA-frame, HDOP and VDOP values as well as sampling time. This data will be called the onboard estimate. From this, an estimate of the variance in each direction can be made to reference that of the raw data as well as a relative estimate of the positions.

### 3.1.5 Global and relative position estimates from raw data

The method for how the positioning is made in the individual as well as the relative case using the log files is presented in the following section. The solutions have only been implemented based on log files and are not made to run real-time. The solution is calculated in two steps:

1. Load the data from log files into an array with a struct for each epoch.
2. Calculate the solution per epoch from the observation and ephemeris data

#### 3.1.5.1 Global positioning

The positioning of each receiver only utilizes the ephemeris data collected by the same receiver and only observation data that has a corresponding ephemeris reading is used. The method for positioning which is implemented follows the description in section 2.5. The solution is an instantaneous estimate for each epoch, indicating that the previous estimate is not taken into account for the current one. This will produce a solution calculated in an ECEF coordinate frame, which is then projected to a NED frame. The solution includes a global position, calculated as described in section 2.5.1 with the weighted estimator of equation 2.26, an estimate of the HDOP and VDOP values, as described in (2.32-2.33) as well as a variance over the solution, calculated per direction in a NED-frame.

### 3.1.5.2 DD relative positioning

For the double difference relative positioning algorithm, **not only must the observation data for each epoch match that of the ephemeris data**, but also must be equal between receivers. For each epoch, any data not contained in both is discarded. **The position must always be calculated using one of the receivers, which will be called  $r_a$ , as reference, and the other, called  $r_b$  fitted to it.** This method, which follows the **instructions** for double difference in section 2.7 utilizes that **clock error cancels out and will not estimate either**. The satellite position is instead calculated at the nominal time of observation  $t_{rec}$ . This is due to the angular change, as opposed to the position change, between satellite and receiver is negligible within the time frame of a sample.

The relative position estimate also requires the receiver position  $p_a$  in order to calculate the unit vector  $e^i$  pointing to a satellite from a receiver. The position used is that given by the onboard estimate. The system of equations is then solved for the given reference satellite, which will be selected as that with the highest SNR value for each epoch, as suggested in [6]. The solution will give an instantaneous relative positional estimate for  $r_b$  with regards to  $r_a$  in an ECEF frame, which is then projected down to a NED solution through the point given. **This also implies that a global position is never calculated through this method.** Given that the receivers were stationary, the estimates are expressed as a mean and a standard deviation in each direction.

## 3.2 Simulation of data

Simulations of data are performed in order to verify the theoretical behaviour of the models under the influence of different noise levels. The theoretical behaviour is then compared to the observations using different levels of bias.

### 3.2.1 Testing different error sources impact on global position

The methods of global positioning and **double difference's behaviour** are also tested using simulated data to verify the theoretical behaviour of the estimator compared to that of the actual measurements. The simulations are based on creating pseudorange measurements between a stationary point on earth and corrupting it with noise, where actual receiver positions are used, and satellites

are positioned according to the orbits from the data contained in the ephemeris messages.

The simulations cover the error sources mentioned in section 2.2 except for the atmospheric noise. From this, a theoretical variance can be derived based on the different error sources of the real sample series and identify potential errors in the estimate method.

### 3.3 RMSE of relative position from global position and DD estimate

Since the DD-method has been shown to improve the relative estimate, mentioned in section 1.6, the assumption is made that the DD-method is superior to that of two individual global fixes in mitigating the effect of a bias. The behaviour is simulated using increasing levels of bias. This means that any two simulated observation between a satellite and the receivers will be of the form

$$y_a = \|\mathbf{p}^{(i)} - \mathbf{p}_a\| + c\Delta t_a + \eta^{(i)} + \epsilon_a \quad (3.1)$$

$$y_b = \|\mathbf{p}^{(i)} - \mathbf{p}_b\| + c\Delta t_b + \eta^{(i)} + \epsilon_b. \quad (3.2)$$

which type of bias?

The notation is consistent with that above. In the simulations, the shared non-white noise  $\eta^{(i)}$  is randomly sampled and will be constant per satellite for the observation series. The simulations are then performed using increasing magnitudes for the bias level. The result is then presented as the root mean square error (RMSE) of the estimate, defined as

$$\begin{aligned} e_{RMS} &= \sqrt{\sum |\mathbf{d} - \hat{\mathbf{d}}|/n} \\ &= \sqrt{\frac{1}{n} \sum_{i=k}^n (\mathbf{d} - \hat{\mathbf{d}}[k]) \cdot (\mathbf{d} - \hat{\mathbf{d}}[k])^T} \end{aligned} \quad (3.3)$$

for a true baseline vector  $\mathbf{d}$  and the corresponding estimated distance  $\hat{\mathbf{d}}[k]$  for an epoch  $k$ . Since the experiment is conducted using the north and east direction separation, the baseline vector will be set to respectively  $[10, 0, 0]$  m and  $[0, 10, 0]$  m.

# **Chapter 4**

## **Results**

### **4.1 Error and convergence from simulated data**

Data is produced through simulations with different kinds and magnitudes of noise. Two kinds of results are presented:

- The convergence of a simulation from an erroneous initial position, erroneous initial receiver clock bias and both an erroneous initial position and receiver clock bias.
- The trend of error in final convergence value for an increasing noise of **different kinds**.

The noise types introduced are as follows:

- Noise free
- Receiver clock bias
- Satellite position random noise
- Measurement white noise



### 4.1.1 Convergence of estimate for noise free measurements with different initial error

The results of simulations of the convergence of the state estimates  $\theta$  as a function of the number of iterations is shown in figure 4.1. When adding an error to the initial estimate is tested, the initial estimate  $\theta_0$  will be equal to the true state  $\theta$  plus a random noise in all three components the position of increasing magnitude of 10 to  $10^7$  m.

The simulations were found to converge with an initial state error in the position of magnitude up to  $10^7$  m in all directions. MATLAB uses 16 digits of precision by default, meaning that the error is expected to converge to that precision, these results are assumed to be due to observations being in the range of approximately  $2\sim 3 \cdot 10^7$  m making an observation registered with eight digits of precision. When adding noise to the satellite position, a random noise is added to the satellite position of increasing magnitude from 1 to  $10^3$  m. When adding a random noise is tested, a random noise is added to the observations of increasing magnitude from 1 to  $10^3$  m.

In figure 4.2 the convergence of an erroneous initial state is presented. For any magnitude of initial error in all parameters between  $10^{-10}$  to  $10^5$  m the parameters converge to the correct value within the interruption threshold of the estimator function.

### 4.1.2 Final estimate for added measurement noise of different magnitudes

The results to the error in the terminal estimate of receiver states when adding noise of increasing magnitude is simulated. The result is presented in figure 4.3. In the upper graph, three types of errors are shown:  $|\mathbf{p} - \hat{\mathbf{p}}|$  where  $\mathbf{p}$  is the true position and  $\hat{\mathbf{p}}$  indicates a least-squares estimate, similarly  $|\boldsymbol{\theta} - \hat{\boldsymbol{\theta}}|$ , where the mean square error is given by the sum  $\frac{1}{n} \sum (y - \hat{y})^2$  where a simulated observation is produced as that given in equation (2.3), and thus  $\hat{y}$  is the predicted measurement given the calculated satellite's position and estimated state of the receiver from equation (2.4).

The simulations show that for an error consisting only of receiver clock bias, the effect on the positioning is negligible, as  $|\mathbf{p} - \hat{\mathbf{p}}|$  lies steadily around  $10^{-10}$ . For other types of added noise, the error appear to grow at the same rate as that

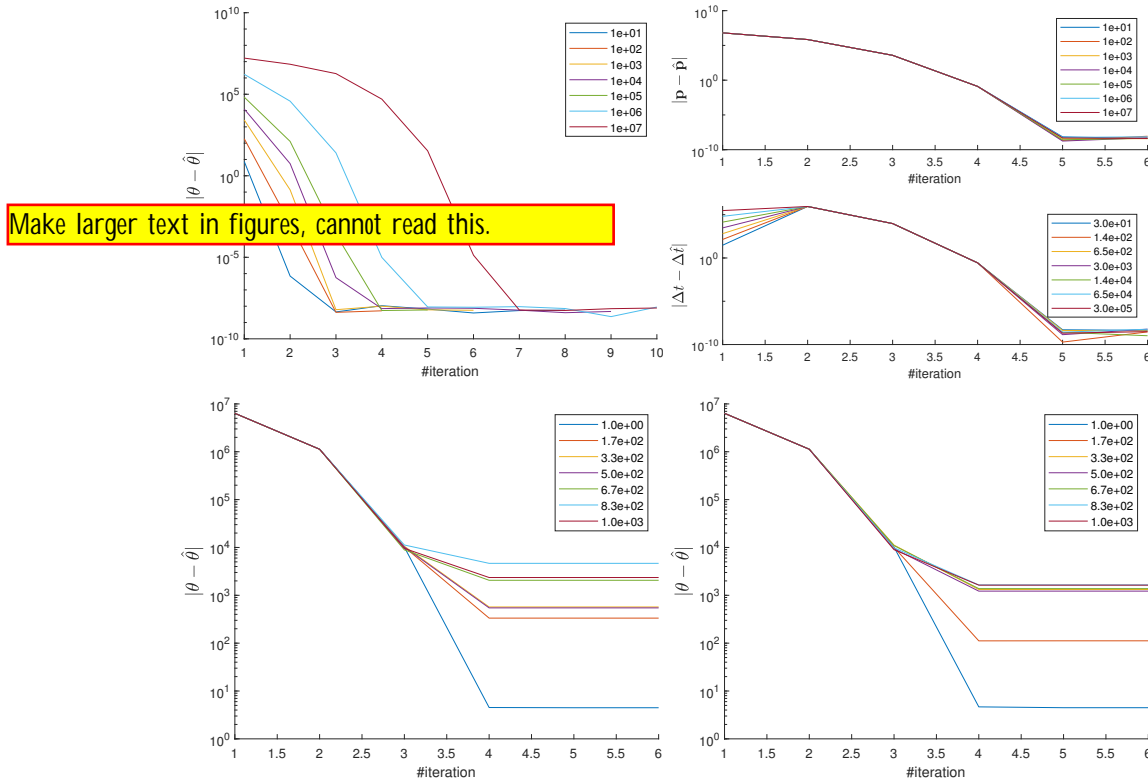


Figure 4.1: Simulation results with different input noise. From top left to bottom right: a) Noise free, b) Clock bias, c) Satellite position, f) Gaussian noise. In figure a), different error in starting positions is tested. The horizontal axis shows the number of iterations and vertical axis shows the norm of the error between true and estimated states  $|\theta - \hat{\theta}|$ .

of the noise source.

## 4.2 Calculating satellite position

The satellite positions are calculated in accordance with the method described in section 2.3. The position is presented in two forms, the position in the sky over time in a polar chart without any corresponding time stamp, as well as 1D graphs of elevation with regards to the position of the receiver given by the onboard electronics. For measurements taken on April 11, 2019, starting at 12:25:28 (UTC), the skyplot of the calculated satellite positions are shown

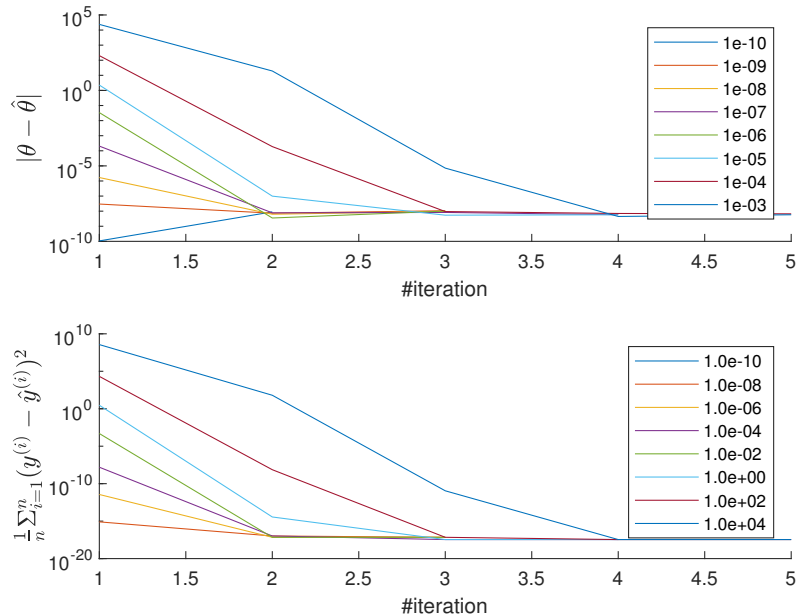


Figure 4.2: The plots show the convergence behaviour with noise free estimates and an initial random error in both position and clock bias of increasing magnitude. Upper: error in  $|\theta - \hat{\theta}|$  per iteration. Lower: mean square error in estimated observation

in figure 4.4, next to that available at online source<sup>1</sup> The elevation, azimuth and distance calculations for the GPS satellites over the same time interval as indicated in figure 4.4 is shown in figure 4.6. The corresponding elevation over time for the satellites in figure (4.5) is shown in figure 4.7. Note that the time interval is larger in figure 4.7 than that of 4.6 due to only actually sampled satellite ephemeris data is used and satellites only being visible for a short time period.

A coarse evaluation indicates that the solutions are equal. The precision with which the satellite positions can be evaluated is however quite low with regards to a fine positioning solution.

---

<sup>1</sup>link to reconstruct plot: <https://www.gnssplanning.com/#/embedded?satellites=1, 2, 3, 5, 6, 7, 8, 9, 10, 11, 12, 13, 14, 15, 16, 17, 18, 19, 20, 21, 22, 23, 24, 25, 26, 27, 28, 29, 30, 31, 32&satSystems=GPS&restoreSats=0&target=settings&cutoffDeg=0&durationHours=6&utcTime=2019-04-11T12:00:00&hgt=10&lonDeg=18.0687918056&latDeg=59.3481576111>

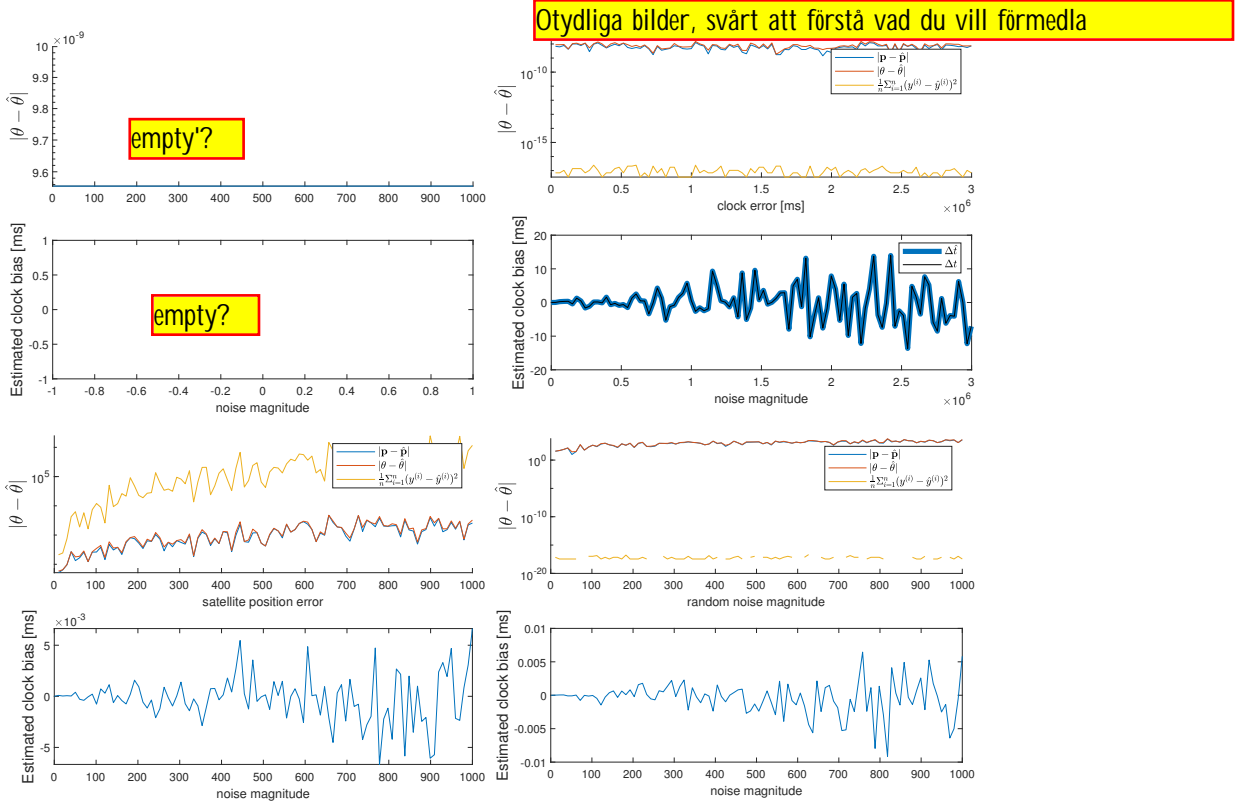


Figure 4.3: Simulation results with different input noise. From top left to bottom right: a) Noise free, b) Clock bias, c) Satellite position, d) Gaussian noise. Note that a) converges to 0 for all iterations. The upper figure in each pair shows the norm of the error in position:  $|\mathbf{p} - \hat{\mathbf{p}}|$ , position+clock bias  $|\theta - \hat{\theta}|$  and expected observation mean square error  $\frac{1}{n} \sum_{i=1}^n (y^{(i)} - \hat{y}^{(i)})^2$  as function of noise magnitude and the bottom figure the calculated clock bias as function of noise magnitude.

### 4.3 Position estimate using global positioning

This section presents the results of the onboard estimate and the individual global positioning. Sampling was performed for approximately 30 minutes per receiver in each direction.

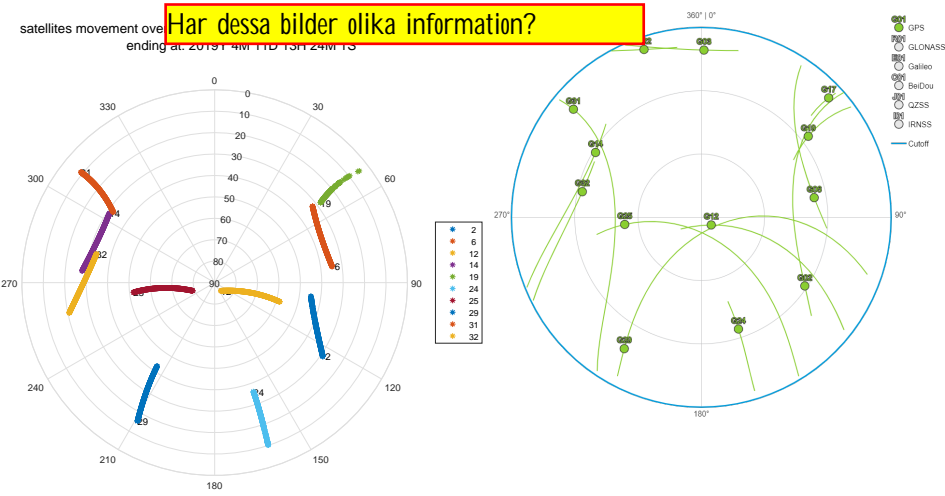


Figure 4.4: GPS Satellite's movement in the sky for the duration of the measurement, only showing when they are observed by the receiver.

Figure 4.5: Skyplot for all visible GPS-satellites at UTC 2019-04-11, 12:30 Stockholm, Sweden from [gnssplanning.com](http://gnssplanning.com). Trajectories indicated without direction

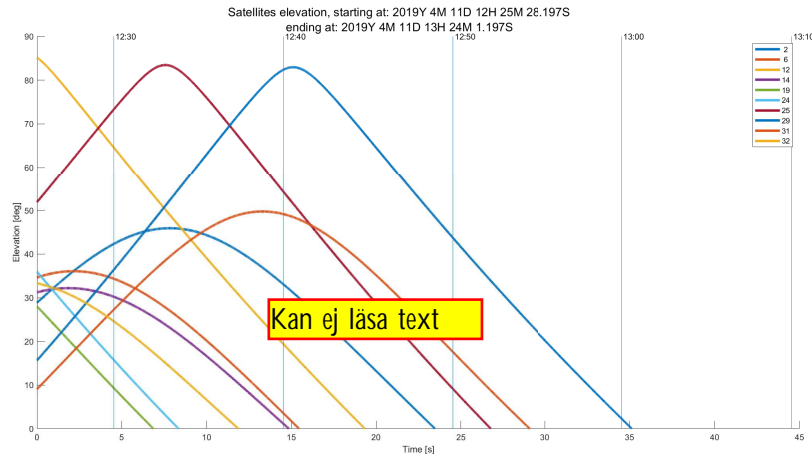


Figure 4.6: Elevation (upper), Azimuth (middle) Distance (lower) for GPS-satellites with regards to receiver at position 59.353°N, 18.073°E.

### 4.3.1 Position from onboard estimate

The result of the two individual estimates is illustrated in figures 4.8-4.9 from a approximately 8500 samples per receiver. The estimate is transformed from

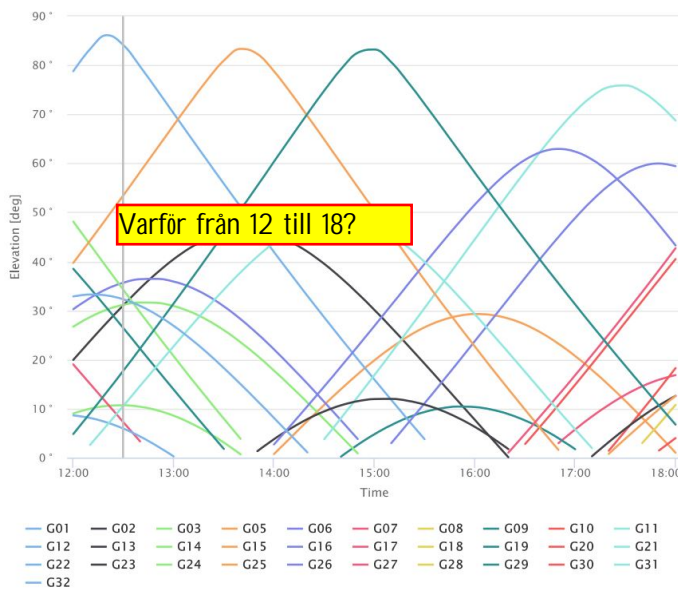


Figure 4.7: Elevation plot from [gnssplanning.com](http://gnssplanning.com) at coordinates 59.353°N, 18.073°E.

an ECEF frame to a NED frame using the first registered position from receiver 1. Here the origin has been set to the mean over time for receiver 1 per direction. The ideal outcome would be positions separated by 10 m in one direction and 0 in the others and have a Gaussian distribution.

The standard deviation per direction and observation series is presented in table 4.1.  $\sigma_{12}$  has been introduced to denote the standard deviation in the relative estimate between the receivers. It is apparent from the images and the data in the table that the standard deviation of receiver 2 is greater than that of receiver 1 for all directions in both observations. It can be noted that receiver 2 is that which was placed close to the pin in figure 3.1 and was closer to the forest right north of it than receiver 1 for both observations.

### 4.3.2 Least square estimator from raw observation data

The global position for two receivers is also calculated as described in section 2.5 using the transmitted ephemeris data to calculate the satellite positions in ECEF coordinates in combination with raw observational data. The observations are weighted using their respective SNR-value as described in equation (2.26). The results are based on approximately 8500 samples per receiver and

Även dessa bilder kan göras större, de är ju redan på varsin sida.

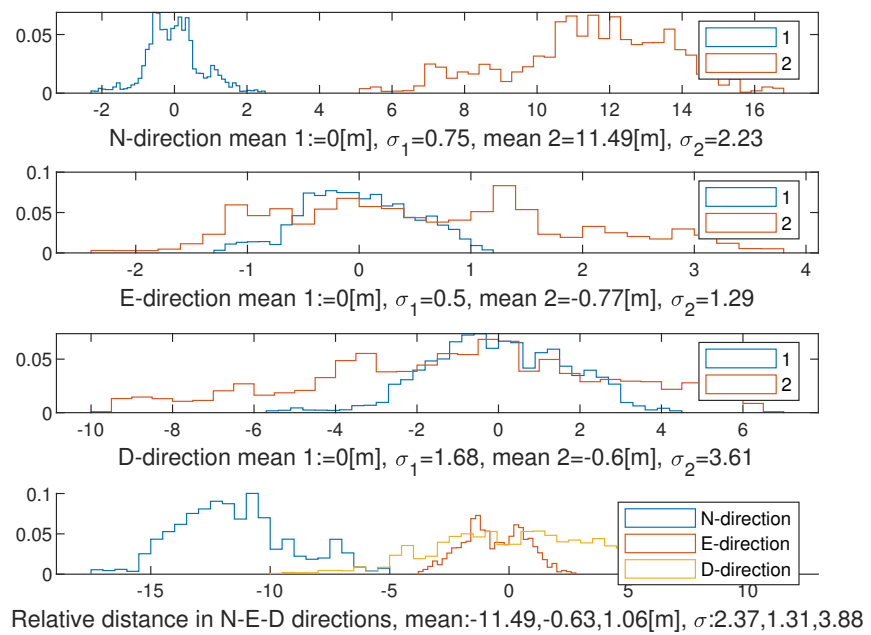


Figure 4.8: Histogram over position over time with an East direction baseline of 10 m separate per direction, N-direction (upper), E-direction (second from top), D-direction (second from bottom), Relative distance for all three directions at synchronised times (bottom)

Add title, which experiment is this?

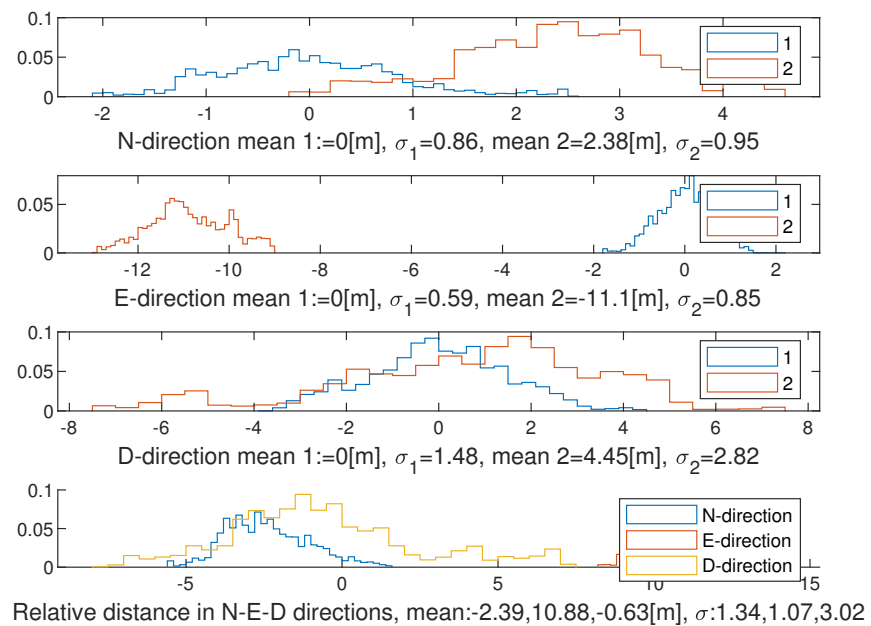


Figure 4.9: Histogram over position over time with an North direction baseline of 10 m separate per direction, N-direction (upper), E-direction (second from top), D-direction (second from bottom), Relative distance for all three directions at synchronised times (bottom)

Add more text here, what are some conclusions? Is this result expected.

The reader should be able to look at a figure and read about the results (almost) independently.

	<b>North</b>	<b>East</b>	<b>Down</b>	
<b>N-dir</b>				
$\Delta p$	-11.5	-0.6	1	Vad är skillnad mellan första och andra mätningarna?
$\sigma_1$	0.8	0.5	1.7	Det är samma vänsterkolumn
$\sigma_2$	2.2	1.3	3.6	
$\sigma_{12}$	2.4	1.3	3.9	
<b>N-dir</b>				
$\Delta p$	-2.4	10.9	-0.6	
$\sigma_1$	0.9	0.6	1.5	
$\sigma_2$	1	0.9	2.8	
$\sigma_{12}$	1.3	1	3	

Table 4.1: Mean and standard deviation of position from on board individual estimate, as well as the relative estimate. Values referring to the figures 4.8-4.9

observation series. They are presented in two ways:

- The positions are calculated independently for the receivers, using all available satellites.
- Only satellites which are shared between receivers are used.

When fully independent estimates are used, several satellites may go in and out of tracking between two epochs, leading to a change in position estimate due to e.g. error in satellite position estimate. The result of fully independent estimates are presented in figures 4.10. The mean and variance, per direction for the two observations are presented in table 4.2.

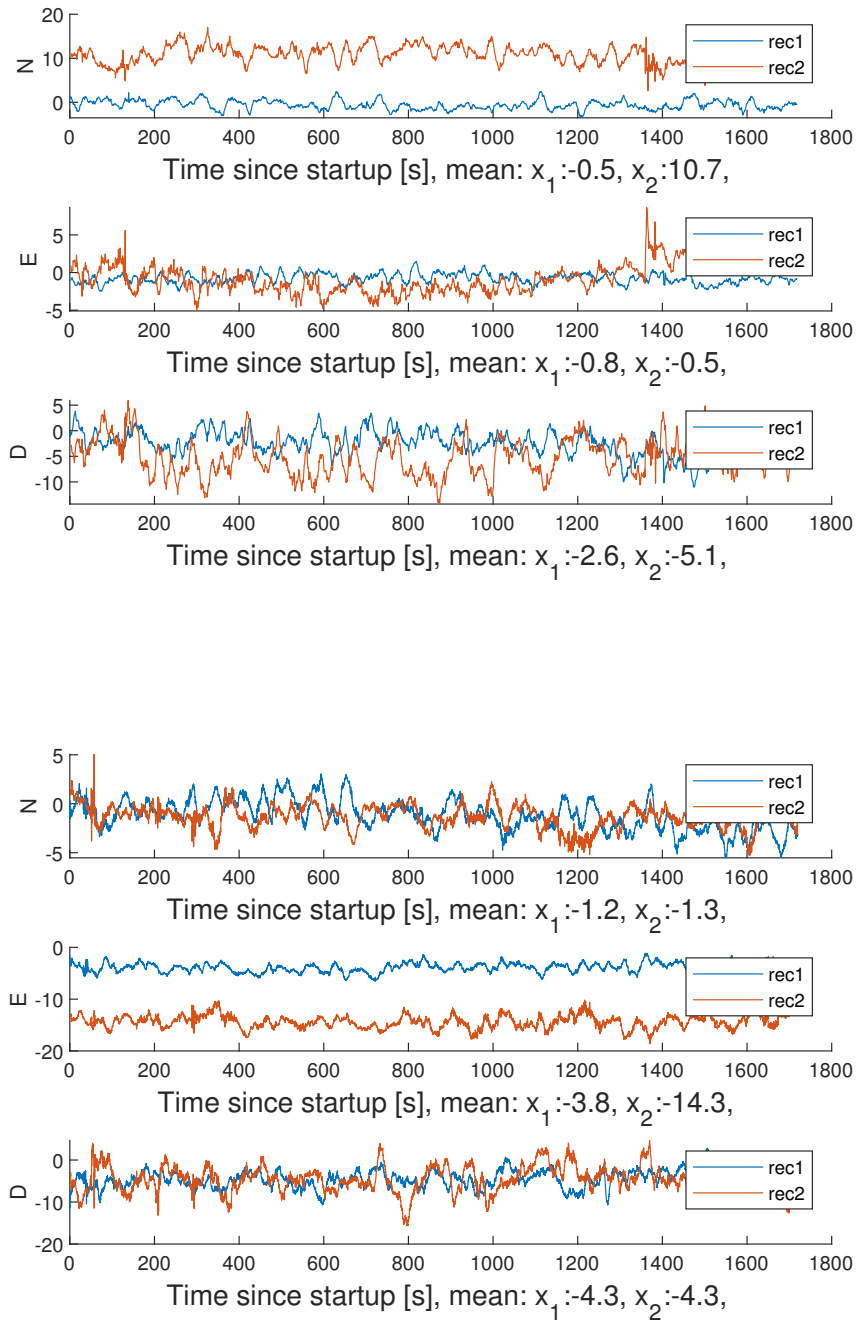


Figure 4.10: Independent global position estimates for two receivers separated 10m N-direction (upper) and E-direction (lower) in N, E and D directions respectively, where the origin is set to true position. All satellite information known to respective receiver is used.

	<b>North</b>	<b>East</b>	<b>Down</b>
E-dir			
$\Delta p$	10.2	0.3	-2.6
$\sigma_1$	1.6	0.9	2.2
$\sigma_2$	1.2	1.3	3.3
N-dir			
$\Delta p$	-0.1	-10.5	0
$\sigma_1$	1	0.7	2.4
$\sigma_2$	2	2.1	3.5

Table 4.2: Averaged values of difference in position and standard deviation of position estimate per direction, receivers use all available rection when only shared satellites information. Values referring to measurements in figure 4.10

	<b>North</b>	<b>East</b>	<b>Down</b>
E-dir			
$\Delta p$	10.6	0.6	-1
$\sigma_1$	1.8	1.4	2.5
$\sigma_2$	1.4	1.3	3.8
N-dir			
$\Delta p$	-1.4	-11.9	-0.4
$\sigma_1$	1	0.7	2.5
$\sigma_2$	2	2.1	3.5

Table 4.3: Averaged values of difference in position and standard deviation of position estimate per direction of position estimate per direction, receivers use all available rection when only shared satellites information. Values referring to measurements in figure 4.11

As a comparison, the position estimate for when only satellites shared between receivers is presented in figure 4.11. This is done by extracting only those satellites which are observed by both receivers from the logged data. The mean and variance per direction for the two observations is presented in table 4.3. The results are very similar but slightly worse for the solution where only shared satellites are used. This leads to the conclusion that this seems to have no positive effect.

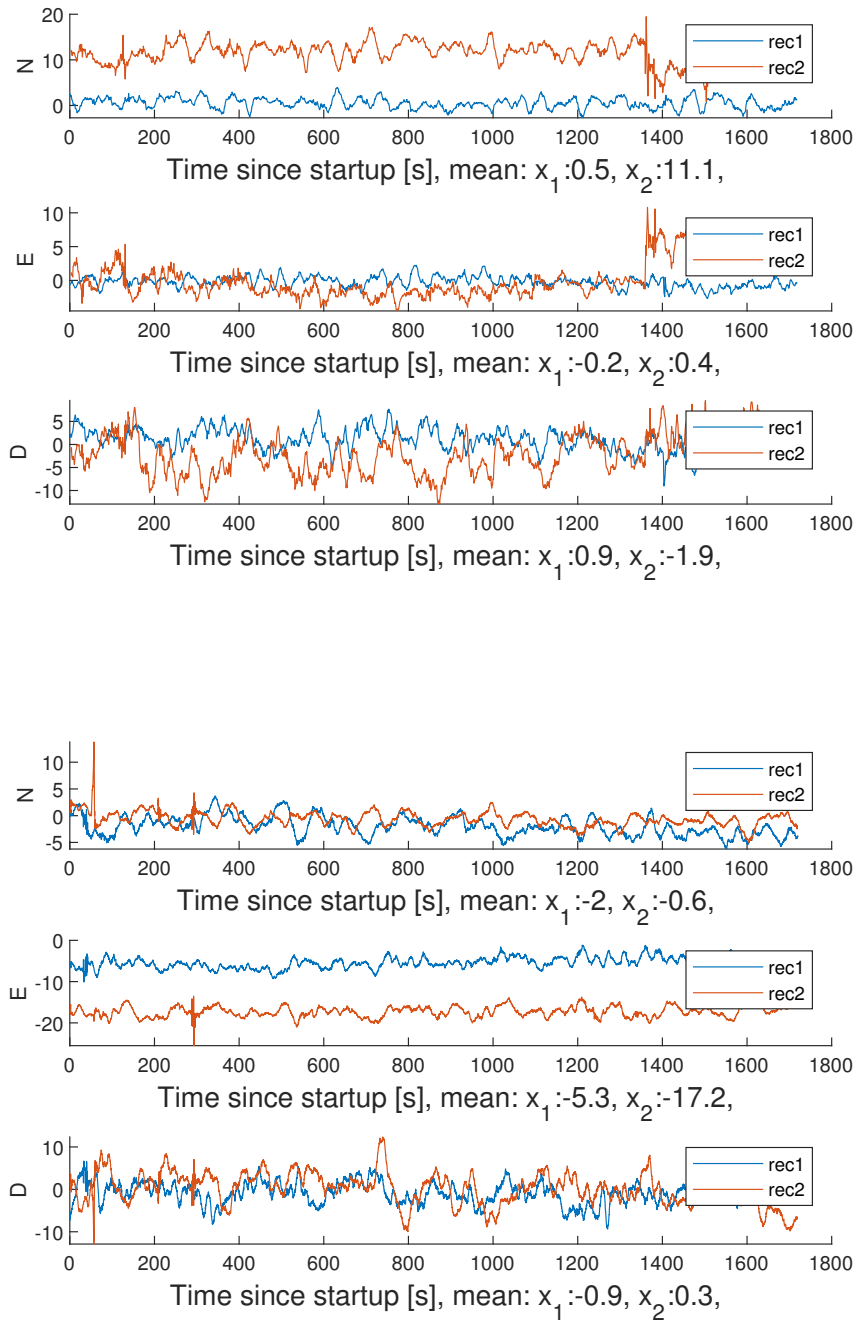


Figure 4.11: Independent global position estimates for two receivers separated 10m N-direction (upper) and E-direction (lower), origin is set to true position. Only satellite data shared between receivers is used.

## 4.4 Relative estimates

### 4.4.1 Histograms of relative position and noise estimates

The same sampling process as above is used, using only the momentary estimate from pseudorange measurements, is shown in figures (4.12-4.13). The mean and standard deviation for each direction of the two sample periods is presented in table 4.4.

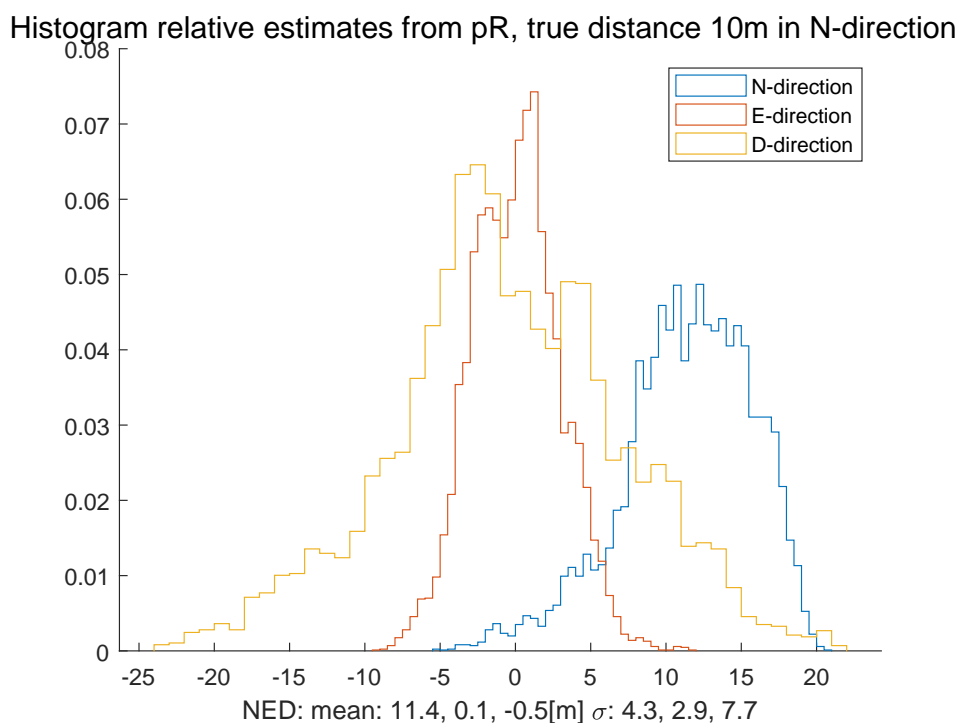


Figure 4.12

The results from section 4.3.1 is compared those presented in figures (4.12-4.13) in figures (4.14-4.15). The plots clearly show that the standard deviation of the DD-estimate at best is equal to, or close to equal to that of the onboard solution but generally can be expected to be greater.

Write in text, what should the value be

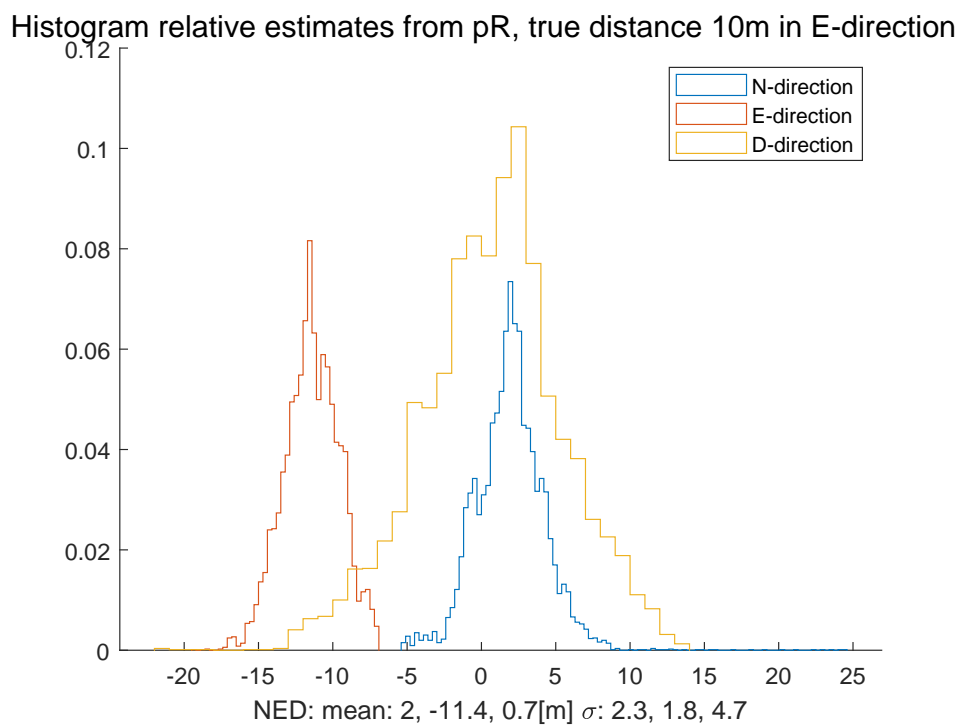


Figure 4.13

	<b>North</b>	<b>East</b>	<b>Down</b>
True[m]	10	0	0
Mean[m]	11.4	0.1	-0.5
$\sigma$	4.3	2.9	7.7
True[m]	0	10	0
Mean[m]	2	-11.4	0.7
$\sigma$	2.3	1.8	4.7

Table 4.4: Averaged values of difference in position and standard deviation of position estimate per direction for a DD-estimate. Values referring to measurements in figure (4.12-4.13)

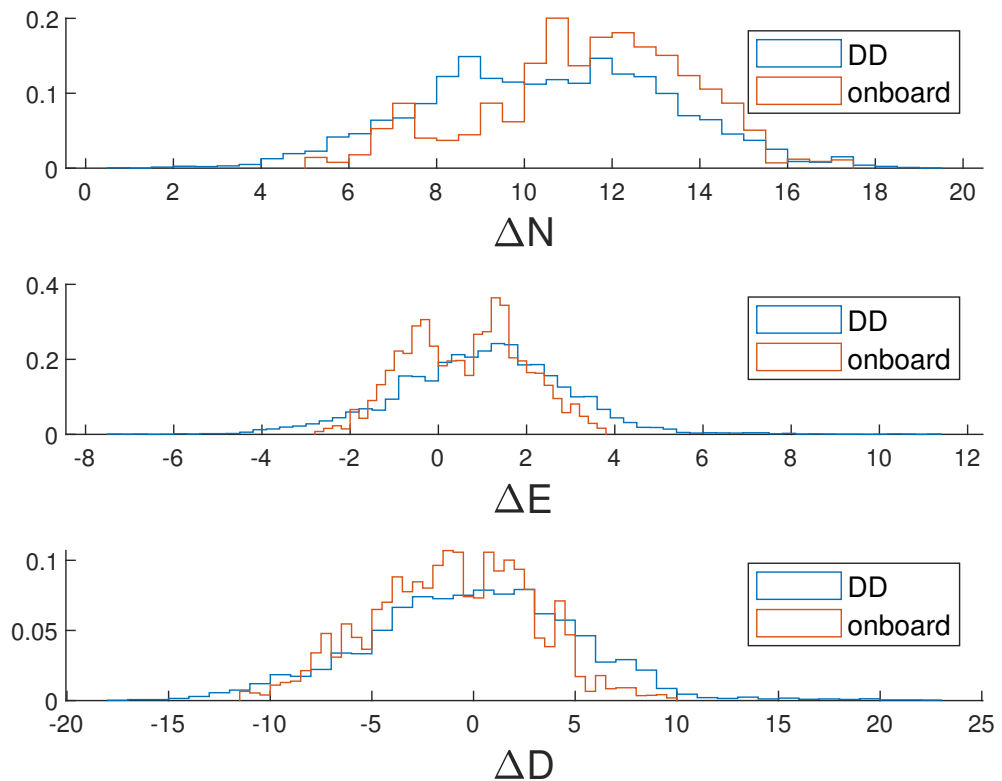


Figure 4.14: Histogram over difference in position over time with a North direction baseline of 10 m. Plots showing results of DD and onboard solution.

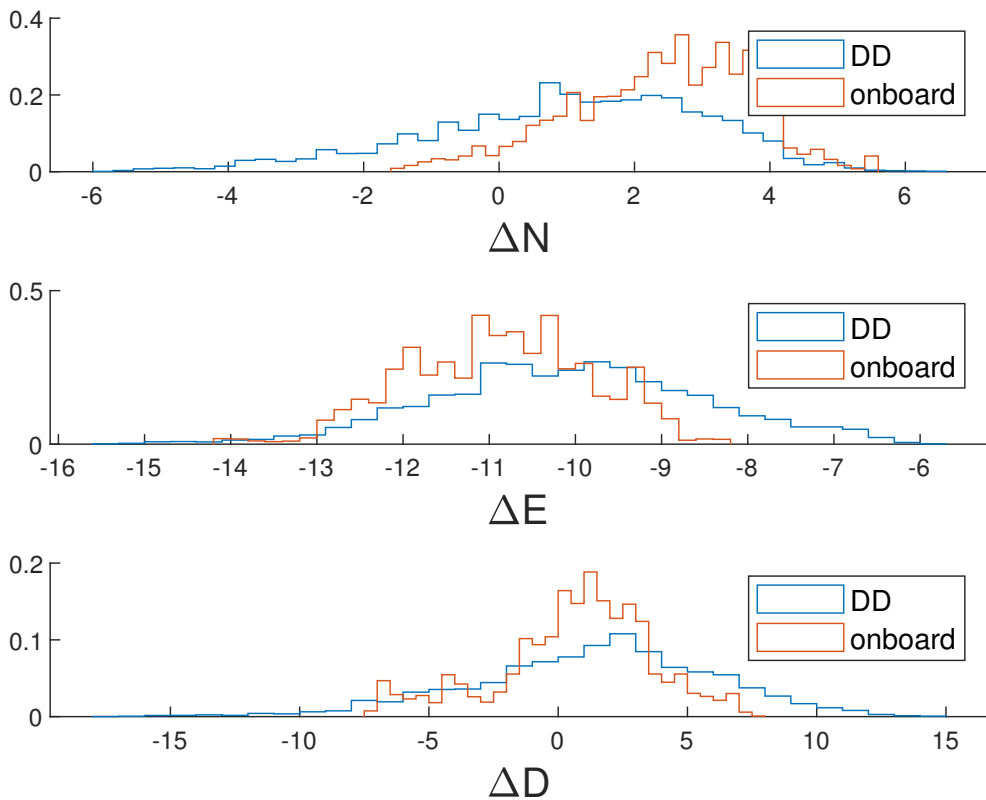


Figure 4.15: Histogram over difference in position over time with an East direction baseline of 10 m. Plots showing results of DD and onboard solution.

## 4.5 RMSE of relative position from global positioning and DD estimate

All the simulations described in section 3.3 are performed using a Gaussian white noise level of 1 m. The positions are then calculated first using two independent global fixes, and then the DD relative position, for increasing magnitude of the bias. In figures (4.16-4.18) the simulated results are shown of increasing the magnitude of the bias which is set to respectively 1, 10 and 20 m. It's apparent that for the global positioning the error grows with the bias, while the differenced position appears to be unchanged which motivates the use of this method for high levels of the common noise  $\nu$  shared between the receivers.

The result of the same calculations performed for the actual observation data is presented in figures (4.19-4.20) with a 10 m separation in north and east di-

Norm of difference in position for simulated data using bias 1

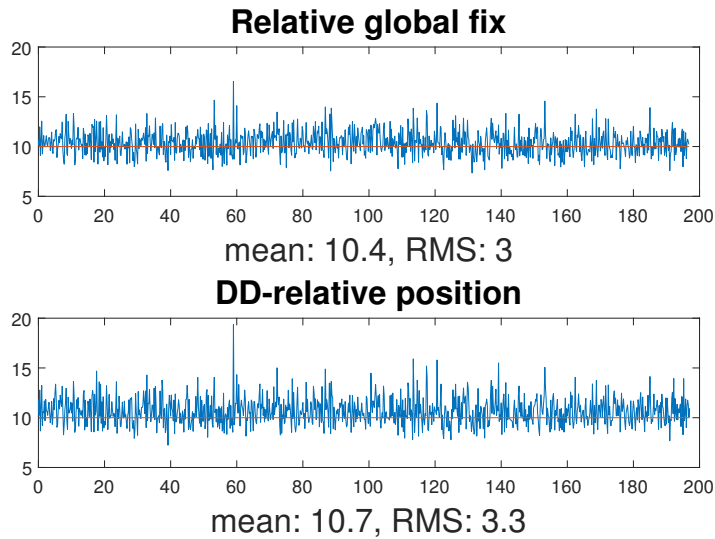


Figure 4.16

Norm of difference in position for simulated data using bias 10

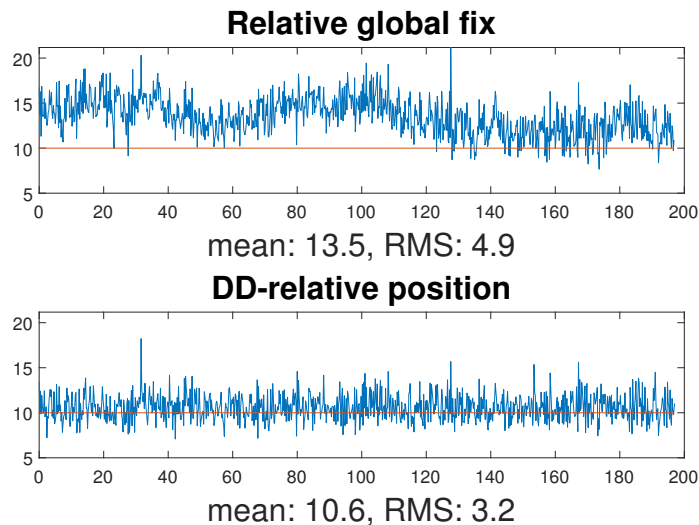


Figure 4.17

rection separation respectively. The calculated RMSE values are, respectively in the north and east direction for the global estimate and DD solutions are 5.6 and 4.9 m in north direction, and 5 and 4.8 for east-direction. The DD-method thus performs slightly better for that of the DD-relative position in both cases.

Men inte på samma sätt som förväntas från simuleringarna.

Norm of difference in position for simulated data using bias 20

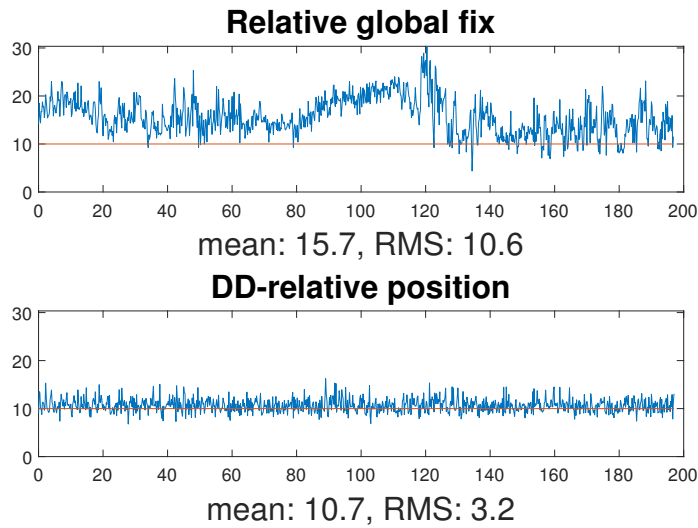


Figure 4.18

## 4.6 DOP values

The DOP-values of the **observations series are** calculated as presented in section 2.8. If the DOP values are poor, then the performance of the estimator can also be expected to be poor. A notable difference between the results of the global estimates and the DD estimate is that the TDOP-value isn't included in the equations for the latter as the receiver bias  $\Delta t_{rec}$  **isn't** estimated. This results in the DOP-matrix being reduced to a  $3 \times 3$  matrix. Besides that, calculations are performed equal to a global estimate DOP-value.

### 4.6.1 DOP values global estimates

In figure 4.21-4.22, the DOP values are presented. The values are quite similar for receiver 1 and receiver 2. With a small baseline distance, only the satellites observed should produce a difference in their DOP values. The HDOP and VDOP value with a mean of around 0.5 and 2 respectively at N-separation observation, and mean of around 0.45 and 1.6 for the E-separation observation. These are all well within the acceptable range of what can be considered good

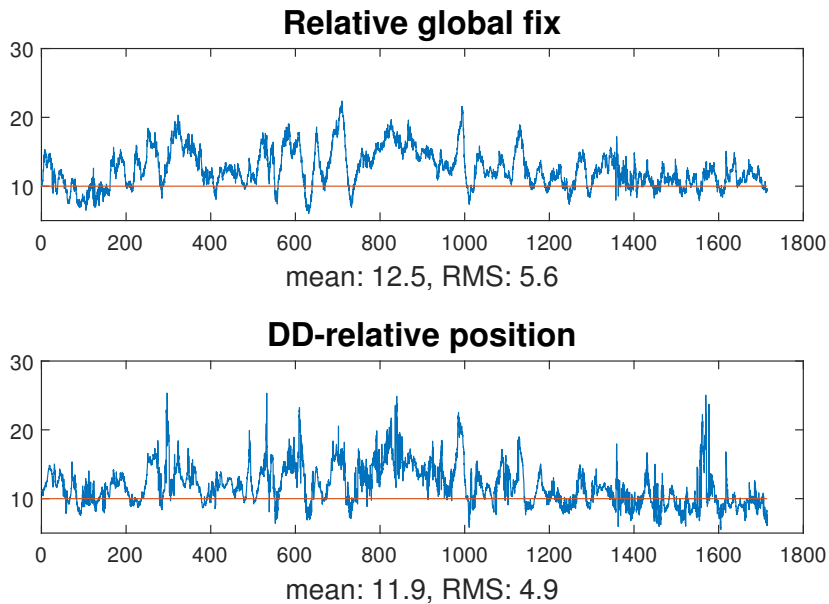


**Figure 4.19:** Result of relative position from global position fixes (upper) and DD relative position (lower) from observation data in a north-direction separation.

geometry, as presented in section 2.8.

### 4.6.2 Double differenced DOP values

In figures 4.23-4.24 the HDOP and VDOP values are calculated as previously mentioned, but only the directional matrix given by 2.30 is used as the clock errors aren't estimated, which only produces an estimate of the geometric uncertainty. The values have a mean at 0.56 for the HDOP and 0.77 for VDOP in the N-direction separated observation, and 0.46 and 0.57 for the E-separated observation. The GDOP value, calculated as

$$q_G = \sqrt{q_H^2 + q_V^2}$$

when the TDOP value is omitted also indicate a very good geometry with the exception of a few samples where it exceeds 3.

What does this mean for your solutions?  
Add reflections on why this matters and how

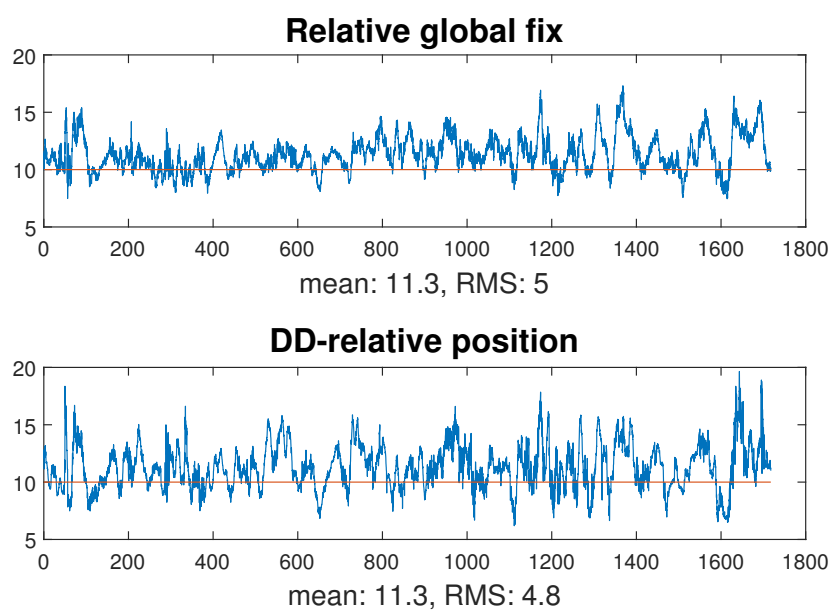


Figure 4.20: Result of relative position from global position fixes (upper) and DD relative position (lower) from observation data in an east-direction separation.

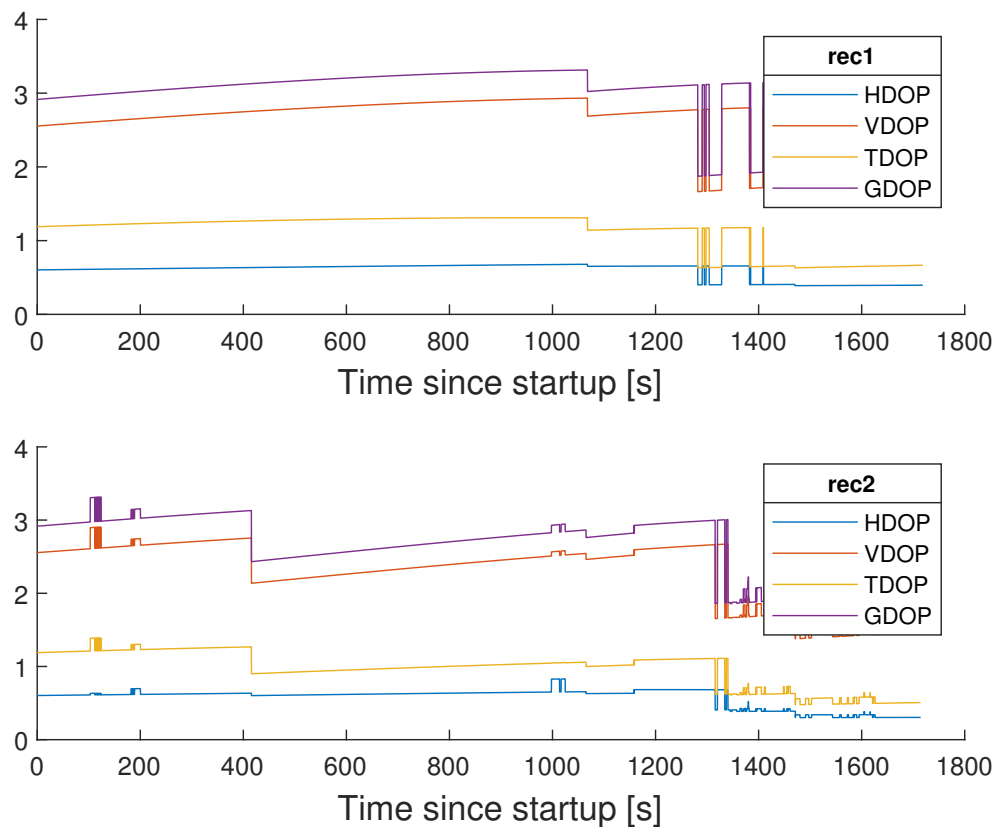


Figure 4.21: Individual DOP values for two receivers separated 10m in N-direction, upper receiver 1, lower receiver 2.

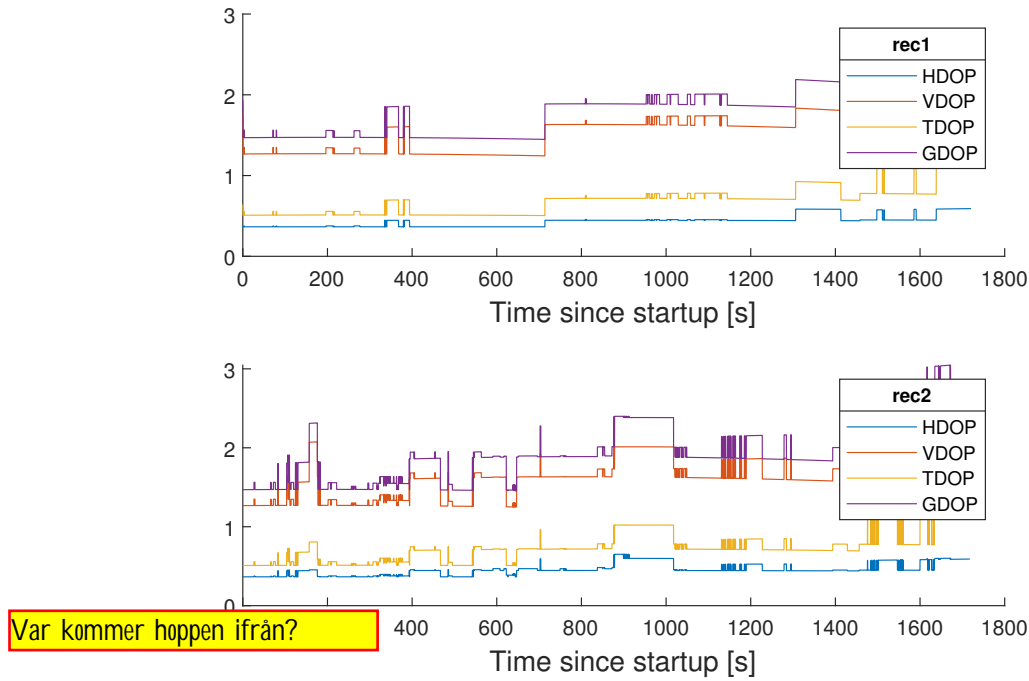


Figure 4.22: Individual DOP values for two receivers separated 10m in E-direction, upper receiver 1, lower receiver 2.

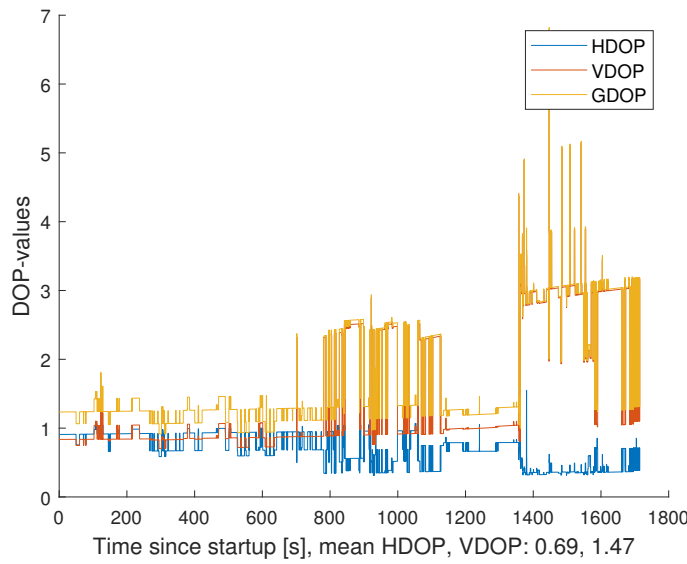


Figure 4.23: DOP values from DD-estimate for two receivers separated 10m in N-direction.

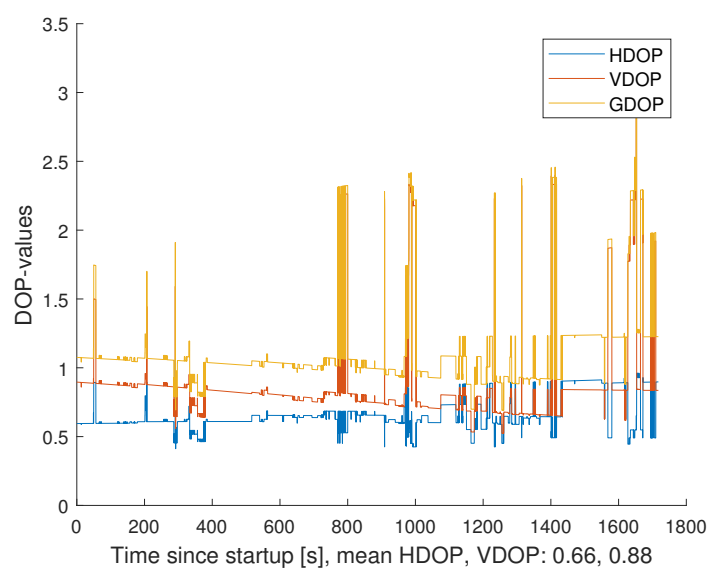


Figure 4.24: DOP values DD-estimate for two receivers separated 10m in E-direction.

# Chapter 5

## Conclusions and further work

### 5.1 Results of simulations

The results of the simulations presented in section 4.1 indicate that the implemented model works as expected as the error in position estimate grows equal to the noise in the input. It also verifies that the use of a DD-approach is meaningful when comparing the RMSE-values of an increasing signal bias, as illustrated in section 4.5. As the error of the DD-method is seemingly unchanged by the bias compared to the relative position of the global estimates, where it grows with increasing bias.

### 5.2 Precision of the estimates

Har detta att göra med mottagarna eller är resultatet allmängiltigt?

The results that have been achieved point towards a slight improvement of an implementation of the DD-method, as compared to that of two individual position estimates. The large variance that was obtained in section 4.4.1 and 4.5 is however unsatisfactory with the ambition to reach below meter accuracy of the estimator. The answer to the question posed at the start of this project posed in section 1.8, seem to be that the noise level may very well be too large to reach the desired precision. The best results are still obtained from the solution directly sampled from the estimate of the onboard solution, as shown in figures (4.14-4.15). Part of the superior performance of the onboard estimate is presumably due to that its estimate is filtered, which can attenuate much of the high-frequency noise and perform outlier rejection. The big dif-

ference in of the noise levels between the two receivers indicated both by the onboard estimate presented in section 4.3.1 as well as the implemented least squares estimate in 4.3.2 is assumed to be an effect of greater noise levels for the receiver placed closer to the forested area. If this assumption is true, the noise levels appear to vary much stronger based on the surroundings than was initially assumed at the beginning of this project.

### 5.3 DOP values

Vad innehåller detta för dina resultat? Att felet borde ligga inom x m?

The results of the DOP-value calculations in section 4.6 indicate that a good geometry of satellites was available for all observations with the exception of a few observations. This comes as no surprise as the receivers had access to observations from more than 10 satellites from all epochs. The DOP-value is an important complement to keep track of in order to avoid situations of very poor geometry but may be of limited use to estimate actual errors as it doesn't contain information on the actual noise levels in observations.

### 5.4 Further work

Two suggestion for further work with regards to the high noise levels discussed in 5.2 are:

1. Implement a filtering process and outlier rejection for the raw observation data.
2. Verify this assumption of noise local noise differences by making observations at a more open place than that used for this project.

The method should also be implemented for real-time use, as the post-processing made only serves a theoretical purpose at the moment. Hopefully, the code which has produced these results can be used as a base for further development of a more useful implementation.

# Bibliography

- [1] Erik Mattias Soop. *Handbook of geostationary orbits*. Vol. 3. Springer Science & Business Media, 1994.
- [2] C. Jeffrey. *An Introduction to GNSSGPS, GLONASS, Galileo and other Global Navigation Satellite Systems*. NovAtel Inc, 2010.
- [3] C. J. Hegarty and E. Chatre. “Evolution of the Global Navigation SatelliteSystem (GNSS)”. In: *Proceedings of the IEEE* 96.12 (Dec. 2008), pp. 1902–1917. doi: 10.1109/JPROC.2008.2006090.
- [4] Leroy O Garciano, Ricky Anderson, and Jan Henrik Reese. “Global Navigation Satellite Systems (GNSS) technologies for Off-Highway Agricultural Vehicles: The Benefits of using State-of-Art Mobile Hydraulics Technology”. In: () .
- [5] Aurello Patrik et al. “GNSS-based navigation systems of autonomous drone for delivering items”. In: *Journal of Big Data* 6.1 (June 2019), p. 53. ISSN: 2196-1115. doi: 10.1186/s40537-019-0214-3. URL: <https://doi.org/10.1186/s40537-019-0214-3>.
- [6] D. Yang et al. “A GPS Pseudorange Based Cooperative Vehicular Distance Measurement Technique”. In: *2012 IEEE 75th Vehicular Technology Conference (VTC Spring)*. May 2012, pp. 1–5. doi: 10.1109/VETECS.2012.6240332.
- [7] K. Liu et al. “Improving Positioning Accuracy Using GPS Pseudorange Measurements for Cooperative Vehicular Localization”. In: *IEEE Transactions on Vehicular Technology* 63.6 (July 2014), pp. 2544–2556. doi: 10.1109/TVT.2013.2296071.
- [8] Jay Farrell and Matthew Barth. *The global positioning system and inertial navigation*. Vol. 61. McGraw-hill New York, NY, USA: 1999.

- [9] Luis Sardinha Monteiro, Terry Moore, and Chris Hill. “What is the accuracy of DGPS?” In: *The Journal of Navigation* 58.2 (2005), pp. 207–225.
- [10] Yanming Feng and Jinling Wang. “GPS RTK performance characteristics and analysis”. In: *Journal of Global Positioning Systems* 7.1 (2008), pp. 1–8.
- [11] Nie Jianhui, Qi Jianzhong, and Song Peng. “Research of GNSS real-time pseudorange differential positioning technology”. In: *International Conference on Cyberspace Technology (CCT 2013)*. Nov. 2013, pp. 370–375. doi: 10.1049/cp.2013.2156.
- [12] J. A. Klobuchar. “Ionospheric Time-Delay Algorithm for Single-Frequency GPS Users”. In: *IEEE Transactions on Aerospace and Electronic Systems AES-23.3* (May 1987), pp. 325–331. issn: 2371-9877. doi: 10.1109/TAES.1987.310829.
- [13] SDP Williams and FG Nievinski. “Tropospheric delays in ground-based GNSS multipath reflectometry—Experimental evidence from coastal sites”. In: *Journal of Geophysical Research: Solid Earth* 122.3 (2017), pp. 2310–2327.
- [14] Malek Karaim, Mohamed Elsheikh, and Aboelmagd Noureldin. “Chapter 4 GNSS Error Sources”. In: 2018.
- [15] Ekrem Tusat and Fethi Ozyuksel. “COMPARISON OF GPS SATELLITE COORDINATES COMPUTED FROM BROADCAST AND IGS FINAL EPHEMERIDES”. In: *International Journal of Engineering and Geosciences* (Feb. 2018), pp. 12–19. doi: 10.26833/ijeg.337806.
- [16] Michael J Dunn and DAF DISL. *Global Positioning System Directorate Systems Engineering & Integration Interface Specification IS-GPS-200*. 2012.
- [17] F. K. Brunner, H. Hartinger, and L. Troyer. “GPS signal diffraction modelling: the stochastic SIGMA- $\delta$  model”. In: *Journal of Geodesy* 73.5 (June 1999), pp. 259–267. issn: 1432-1394. doi: 10.1007/s001900050242. url: <https://doi.org/10.1007/s001900050242>.
- [18] Geoffrey Blewitt. “Basics of the GPS technique: observation equations”. In: *Geodetic applications of GPS* (1997), pp. 10–54.

- [19] Mahdia Tahsin et al. “Analysis of DOP and its precision in GNSS position estimation”. In: *2015 International Conference on Electrical Engineering and Information Communication Technology (ICEEICT)*. IEEE. 2015, pp. 1–6.
- [20] Dmitry Tatarnikov and Andrey Astakhov. “Approaching millimeter accuracy of GNSS positioning in real time with large impedance ground plane antennas”. In: *Proc. ION ITM* (2014), pp. 844–848.
- [21] Richard B Langley et al. “Dilution of precision”. In: *GPS world* 10.5 (1999), pp. 52–59.
- [22] H. Azami, M. Azarbad, and S. Sanei. “New applied methods for optimum GPS satellite selection”. In: *2013 3rd Joint Conference of AI Robotics and 5th RoboCup Iran Open International Symposium*. Apr. 2013, pp. 1–6. doi: 10.1109/RIOS.2013.6595308.
- [23] William R Moser. *Linear models: A mean model approach*. Elsevier, 1996.

NEW PAGE

## .1 Least Squares and Probability

punkt före siffran?

In this section a few fundamental terms regarding the probabilistic distributions which are being used are presented.

### .1.1 Least squares

Assuming that  $A$  is a matrix of size  $m \times n$ , where the rank is at least  $n$ ,  $\mathbf{x}$  a vector of parameters and  $\mathbf{b}$  a vector of outputs, then the set of equations are expressed as

$$A\mathbf{x} = \mathbf{b}.$$

If  $m > n$ , the equation

$$A\mathbf{x} - \mathbf{b} = 0$$

generally doesn't have a solution. Instead, a cost function  $Q$  expresses the square error of the system, defined as

$$Q = (\mathbf{y} - A\mathbf{x})^T(\mathbf{y} - A\mathbf{x}) \tag{1}$$

$$= \mathbf{y}^T\mathbf{y} - 2\mathbf{x}^T A^T A + \mathbf{x}^T A^T A \mathbf{x}. \tag{2}$$

The vector  $\hat{\mathbf{x}}$  is the parameters which minimizes the norm of  $Q$ , which is expressed as

$$\hat{\mathbf{x}} = \underset{\mathbf{x}}{\operatorname{argmin}}(||\mathbf{y} - A\mathbf{x}||). \quad (3)$$

The solution to 3 is found through finding the zeros to the derivative of  $Q$  with respect to all parameters in  $\mathbf{x}$ ,

$$\frac{\partial Q}{\partial \mathbf{x}} = -2A^T\mathbf{y} + 2A^TA\mathbf{x} = 0$$

which is where

$$A^T\mathbf{y} = A^TA\mathbf{x}. \quad (4)$$

for some value  $\hat{\mathbf{x}}$ . Multiplying both sides with the inverse to  $A^TA$  and thus the least square solution is given as

$$\hat{\mathbf{x}} = (A^TA)^{-1}A^T\mathbf{y} \quad (5)$$

$$(6)$$

### **.1.1.1 Weighted Least Squares**

This can be extended to a more general case to capture the uncertainties of the individual measurements. Assume that the matrix  $W$  contains the variances of the noise and is a diagonal matrix defined as

$$W = \begin{bmatrix} \sigma_1^2 & 0 & \dots \\ 0 & \sigma_2^2 & 0 \\ \vdots & \ddots & 0 \\ 0 & \dots & 0 & \sigma_m^2 \end{bmatrix}. \quad (7)$$

Then a Best Linear Unbiased Estimator (BLUE) estimation can instead be given by:

$$\hat{\mathbf{x}}_{BLUE} = (A^TW A)^{-1}A^TW\mathbf{y} \quad (8)$$

The full derivation of the BLUE model can be found in [23].

### **.1.2 Data structs and log format**

The INS unit provides several possible struct types of information which can be sampled at different frequencies depending on the type, where GNSS-signals

can be sampled at up to 5 Hz, while the IMU offers sampling up to 250 Hz. Among them there are both relatively unprocessed as well as processed data. A few data structs have been sampled from in this project and will be described briefly:

- `ins_1_t` - Fused data from IMU and GNSS sensors, including position (LLA/NED), velocity (body frame) and sampling time.
- `gps_pos_t` - Pure GPS receiver processed data, including global position (ECEF/LLA), DOP, and sampling time.
- `gps_raw_t` - Raw observation data, including number of observations, data and data type (needed for the following fields).
- `obsd_t` - Raw observation data, contains receiver sampling time, satellite number, SNR (0.25dBHz), observation data carrier phase and observation pseudorange.
- `eph_t` - Satellite ephemeris data, contains information on satellite number, time of data transmission and time for ephemeris data issue, as well as all data mentioned in section 2.3.

The sampled data is saved in separate logs for each receiver for later processing. For the ephemeris log file the format is a single row for each observation including time of reception. For the observation data, the data in each epoch comes in a package of multiple observations. One whole package of observation will be logged in one row, with number of observation, time of reception shared for all followed by satellite data, SNR, loss of lock indicator, code indicator and observation data repeated in the following format:

```
#obs, time1, time2, [satNo, SNR, LLI, code, P], [satNo, SNR, ...]
```

e.g.

```
2,1562426103,0.391000,22,112,2,1,21772765.735608,41,76,0,1,20961030.484006,
```